ENGINEERING BIOMATERIALS-BASED APPROACHES FOR BETTER ANGIOGENESIS

By

SUE HYUN LEE

Dissertation

Submitted to the Faculty of the

Graduate School of Vanderbilt University

in partial fulfillment of the requirements

for the degree of

DOCTOR OF PHILOSOPHY

in

Biomedical Engineering

May, 2016

Nashville, Tennessee

Committee Members:

Mark D. Does, Ph.D.

Todd D. Giorgio, Ph.D.

Melissa C. Skala, Ph.D.

Leon M. Bellan, Ph.D.

David M. Bader, Ph.D.

Acknowledgement

This work was made possible in large part thanks to Dr. Hak-Joon Sung. I cannot thank him enough for challenging me in every way imaginable and providing me with extraordinary and rare learning opportunities and life lessons that extend beyond science, with ample opportunities to question and challenge my beliefs and understanding of the social constructs and governing principles. I could definitely say I've had an extraordinary training, and I expect these lessons to guide me well through the rest of my life. Additionally, I owe it to Dr. Pampee Young, Dr. Ki Dong Park, Dr. Leon Bellan who contributed to this work, as well as various funding sources (NSF CAREER CBET 1056046 and AHA PRE25360026) that supported this work.

I must thank all of my labmates Angela Zachman, Spencer Crowder, Dan Balikov, Tim Boire, Ricky Rath, Mukesh Gupta, Jung-bok Lee, and Lucas Hofmeister, as well as undergraduate students Amy Hwang, Anna Hwang, Frank Schumacher, Jessica Kim and Ian Baird for their friendship, support and collaboration that really enabled this work and introduced me to many interesting projects. I'd also like to acknowledge the close friendship, bottomless support and honest advice that Amy Shah and Kelsey Beavers provided throughout our graduate school journey together, as well as Dr. David Bader and Dr. Todd Giorgio who have provided unwavering support and well-balanced guidance through the most difficult times. These individuals were absolutely critical in the completion of this work and my Ph.D, and I am eternally grateful.

And now, last but not least, I'd like to acknowledge the endless love and support my family has provided me over the years. They surely have been through this wild and expensive ride with me, often playing as the devil's advocate. I hope to pay them back by becoming a respectable, productive and happy adult who positively contributes to society.

Table of Contents

Chapter **Page**

List of Figures & Tables

Chapter 1

Introduction and Motivation

Advancements in stem cell biology, material science, chemical engineering, and regenerative medicine have come together in recent years to give rise to the field of tissue engineering with a vast potential to treat numerous medical conditions. However, a common roadblock holds back most of the tissue engineering applications today from being translated in the clinic: the inability to engineer vascularized constructs that would anastomose with the host circulation. Blood flow is absolutely necessary for the survival of most tissues, and this challenge must be addressed for successful translation of tissue engineering. Specifically, two objectives must be met to address this issue. First is to engineer biomaterials that are conducive to robust angiogenesis, and the second is to find an accessible cell source that would provide the necessary vascular cells for functional vasculature. This work aims to address both of these objectives through the following aims:

Aim 1. Characterize ROS-cleavable oligoproline crosslinked polycaprolactone for pro-angiogenic host response. A reactive oxygen species (ROS)-degradable scaffold was fabricated by crosslinking biocompatible, hydrolytically-degradable poly(ε-caprolactone) (PCL) with a ROS-degradable oligoproline peptide, KP_7K. The motivation behind this approach was the hypotheses that "smart" biomaterials that can interact with host tissue would encourage better integration via better host cell infiltration and angiogenesis, and that implantation would cause localized increase in ROS that could be leveraged. We expected that ROS-mediated degradability of our scaffolds would trigger favorable host responses with improved cell infiltration and angiogenesis *in vivo*.

Aim 2. Characterize MSC behavior in *in situ* crosslinkable gelatin-derived hydrogel *in vitro* and *in vivo*. In order to develop thermally stable gelatin-derived hydrogels for *in vivo* applications, injectable, *in situ* crosslinkable gelatin hydroxyphenyl propionic acid (GHPA) was synthesized. The chemical and mechanical properties of GHPA hydrogels were characterized. This work was largely motivated by our earlier findings where MSCs spontaneously differentiated into endothelial cells when cultured in GHPA *in vitro*. Mesenchymal stem cells (MSCs) were embedded and cultured in 3D GHPA *in vitro* over 15 days, and their interactions within GHPA in terms of viability, morphological changes, gene expression and protein expression were investigated. Additionally, subcutaneously delivered GHPA hydrogels loaded with MSCs were implanted in mice for 2 weeks, and MSC engraftment, angiogenesis, and differentiation *in vivo* were investigated.

Aim 3. Elucidate cell-matrix interactions associated with the gelatin hydrogel that drives MSC transdifferentiation to endothelial-like cells and human MSC response. Studies have shown the various functions of integrins and their downstream signaling that affect cell proliferation, motility, survival, morphology and differentiation. Hence, we first aimed to determine integrin types that are responsible for MSC - GHPA interactions. We then aimed to identify key signaling pathways involved in the vasculoconductive function of identified integrin types and their involvement in the transdifferentiation process using selective inhibitors against signaling cascade components of interest. Defining such signaling pathways will provide new insight into the translational potential of gelatin hydrogels as well as provide more basic understanding of MSCs in developmental and regenerative contexts. Additionally, in order to further examine the translatability of our platform, we applied human patient-derived MSCs (hMSCs) and examined how hMSCs respond to GHPA gel and also their angiogenic potential *in vivo*.

Chapter 2

Background

This chapter is taken in part from:

Lee, Sue Hyun, et al. "Current Progress in Reactive Oxygen Species (ROS)-Responsive Materials for Biomedical Applications." *Advanced Healthcare Materials* 2.6 (2013): 908-915.

2.1 Tissue Engineering for Unmet Clinical Needs

Donor organ shortage is an aggravating, chronic issue: While the field of medicine has experienced magnificent advancements in the last few decades with continuously increasing average life expectancy, the demand for organ donors also continues to rise and remains unfulfilled by a large margin. In the US, there are on average 79 transplants every day, however, an average of 22 patients also pass away from the donor organ shortage every day.[44] In 2013, there were > 120,000 patients waitlisted for transplantation but only about 29,000 transplants have been performed, highlighting the gravity of donor organ shortage issue, which is expected to worsen in the coming years.[44] In addition, the problem is compounded by the fact that organ transplantation has numerous limitations.

Organ transplantation may not be the best solution: First, organ transplantation requires a long-term use of immunosuppressive drugs in order to avoid transplant rejection. Continued use of such drugs has been shown to increase risks for cardiovascular disease, infection and malignancy.[46] Secondly, while immunosuppressive drugs and other improvements in the transplantation techniques have proven successful in dramatically improving the short-term graft survival rate – for example, renal allograft survival rate for the first 12-month improved from 45% to over 95% - this had minimal effect on the long-term graft survival rate, which remains poor.[45] Thus, even if the donor organ shortage problem is mitigated, it is likely that a sizable portion of the patients who receive transplants

would face significant medical issues over time due to failing transplants as well as other increased risks from long-term immunosuppressive drug use. These limitations demonstrate clinically unmet needs that may benefit greatly from successful clinical translation of tissue engineering.

Tissue engineering has started to enter the clinic: With the goal of regenerating functional tissues and organs via purposeful engineering of cells and scaffolds, tissue engineering is slowly becoming a reality in the clinic in recent years, and significant advancements are greatly anticipated as the standard of living and life expectancy continue to improve with an ever increasing clinical need for replacement organs. While no FDA-approved tissue engineering applications exists today, few high profile, experimental approaches have taken place for patients in various life-threatening conditions. Notable examples include 6 trachea implantations led by Dr. Paolo Macchiarini since 2008.[1-6] While the details of each surgery vary, new tracheas were made with either a donated trachea or a trachea made of synthetic material seeded with patients' bone marrow-derived mesenchymal stem cells that could differentiate into cartilage cells. Recent ethical issues aside, the first two trachea implantations remain successful and functional to date, dramatically improving the lives of those patients, while the remaining four trachea implantations have eventually resulted in fatal failures. As seen in these examples, while there are several challenges that must be overcome, tissue engineering is slowly entering the clinic.

Successful tissue engineering requires vascularization and anastomosis with the host: It is not a coincidence that the few aforementioned examples in human patients have been with engineered trachea, which is a relatively avascular organ along with other cartilages and cornea.[7,8] Most other tissues and organs in human body require extensive vascularization every few microns in order to keep the tissues and organs alive and functional through the supply of nutrients and oxygen and removal of waste products that circulation affords.[9] This requirement for vascularization is a major challenge that applies to most tissue engineering applications, yet without a good solution. This challenge has two aspects: first is a structural/material challenge in fabricating an extensive vascular

network within a scaffold or finding a material that supports robust angiogenesis, and second is a challenge in finding a cell source that provides vascular cells such as the endothelial cells, smooth muscle cells and pericytes that are necessary to form and maintain functional vasculature.[8-11] The rest of this chapter is devoted to providing background information on these two aspects.

2.2 Engineering Smart Biomaterials

Smart, stimuli-sensitive biomaterials show promise with new functions: In the field of biomaterials, much of recent work has been put into developing materials that exhibit specific response to biological parameters under abnormal body conditions and deliver therapeutics in a spatially and temporally controlled manner. These materials aim to take advantage of pathological conditions that are often identified with local abnormalities in an array of biological parameters, such as the pH, temperature, protease activities, or redox balance.[12-14] One such stimulus gaining importance of late is reactive oxygen species (ROS), which is implicated in numerous important pathophysiological events, such as atherosclerosis, aging, and cancer. It has become apparent not only that diverse ROS are overproduced locally in damaged cells and tissues, but that they individually and synchronously contribute to many of the abnormalities associated with local pathogenesis. Therefore, advantages of developing ROS-responsive materials extend beyond site-specific targeting of therapeutic delivery, and potentially include navigating, sensing, and repairing damaged parts of the body by programming changes in material properties. As a preliminary proof of concept study, we hypothesized that ROS-degradable scaffolds would enable better interaction with the surrounding host tissues upon implantation which would cause a localized increase in ROS as typically seen in the implantation site and result in better host cell infiltration and angiogenesis, and this is the focus of Chapter 3 in this work.

ROS-degradable biomaterials can be advantageous *in vivo*: Various stimuli-sensitive biomaterials have been developed in recent years and shown promise to offer specific advantages. In particular, a

similar approach to develop ROS-degradable tissue engineering scaffolds has shown promise in vivo. John Martin *et al.* has incorporated ROS-degradable poly(thioketal) into poly(ester urethane) and implanted porous scaffolds, where dramatically increased cell infiltration was observed for the ROS-degradable scaffold.[47] However, this study did not investigate the angiogenic potential of such scaffolds *in vivo*. On the other hand, the aforementioned thioketal polymer was initially developed as an oral siRNA delivery vehicle to treat various intestinal inflammatory diseases that are accompanied by markedly increased ROS levels in the intestine, which allows for site-specific release of siRNA.[48] Most studies in the literature so far have employed ROS-sensitive biomaterials for drug delivery purposes, which signifies the importance of our work in this dissertation as it is among the first in the field that took an advanced technology and applied to tissue engineering.

Gelatin is promising yet difficult to use *in vivo*: Gelatin, a form of denatured collagen which is a major component of extracellular matrix, can be an ideal material for tissue engineering as it is known for its excellent biocompatibility and biodegradability, as well as adhesiveness for cell attachment, and the lack of immuno/antigenicity.[15] However, the *in vivo* application of gelatin has been limited thus far due to its low upper critical solution temperature that liquefies gelatin at 37°C and quick enzymatic degradation. Accordingly, only few studies so far have aimed at understanding the functional aspect of gelatin for stem cell delivery, despite numerous advantages of gelatin for tissue engineering.[16] For example, a number of studies have employed Gelfoam which is highly crossed gelatin in a sponge form that loses the natural hydrogel-like properties in tissue engineering applications.[49,50,52] Interestingly, Chen et al. have used UV-crosslinkable gelatin methacrylate hydrogels with endothelial cells and mesenchymal stem cells, where the cells formed extensive vascular network *in vitro* depending on the mechanical properties of the hydrogel with increased vascular network formation in softer gels.[51] In this study, mesenchymal stem cells were observed to differentiate into perivascular cells, supporting endothelial cells and lumen formation.

Injectable and *in situ* crosslinkable gelatin is a promising solution: To address these issues, we

have recently developed injectable, *in situ*-crosslinkable gelatin hydrogels.[17] Conjugation of hydroxyphenyl propionic acid to the free amines of gelatin (**GHPA**) enabled rapid H_2O_2- and horseradish peroxide (HRP)-mediated crosslinking. Such modification allowed the use of gelatin as an injectable, thermostable hydrogel with tunable degradation resistance and mechanical properties for *in vivo* applications. GHPA hydrogels demonstrated excellent biocompatibility, tunable mechanical properties, and a marked pro-angiogenic effect by promoting endothelial differentiation of MSCs, resulting in robust neovasculature formation throughout the implants, as well as favorable macrophage responses upon implantation (see Chapters 4 and 5). Another important advantage of gelatin-based materials is its non-immuno/antigenicity *in vivo*, as the harsh gelatin extraction process is thought to remove antigenic moieties on intact 3D collagen fibrils.[18,19] In this work, we found that this gelatin-derived hydrogel can be considered as an unprecedented injectable biomaterial platform that is equipped with the ability to direct endothelial differentiation of bone marrow-derived MSCs both *in vitro* and *in vivo* via purely material-driven signaling pathways. Such biomaterial-driven stem cell differentiation would be preferred to soluble factor-mediated differentiation due to better reproducibility, relatively low economic production cost, reduced spatiotemporal variations, minimized side effects, and the provision of physical and instructive support for tissue regeneration at the target site.

2.3 Stem Cell Therapies and Mesenchymal Stem Cells

Stem cell therapy falls short of promise in clinical trials: While there continues to be a stream of clinical trials utilizing autologous stem cells to treat various vascular/ischemic diseases including peripheral artery disease and myocardial infarction, nearly all studies have resulted in disappointing outcomes.[20,21] At best, some of the treatments attenuated the disease progression, but eventually the degenerative process resumed. Accordingly, there is no evidence of significant revascularization or a decreased amputation rate reported from these trials.[20-22] One contributing factor could be that

of the typical dose of ~10^9 cells of bone marrow mononuclear cells (**MNCs**), less than 2% were $CD34^+/VEGFR2^+$ and were thought to be the putative endothelial progenitor cells (**EPCs**).[23] Thus, considering the fact that MNCs do not readily become endothelial cells (**ECs**), most of the therapeutic effects were likely derived from the trophic nature of the delivered cells, rather than through direct contribution of implanted stem cells to forming new blood vessels (i.e. vasculo/angiogenesis).[24-26] Overall, the results from previous studies suggest limited therapeutic benefits to stem cell therapies.[27] At least, these clinical trials have shown that the injection of autologous cells did not cause a severe immunological response in most patients.

What are the suspected reasons for failure?: Several common critical challenges have been highlighted through these clinical trials testing stem cell-based therapies. First, there is a clear lack of stem cell population with demonstrated angio/vasculogenic potential that would directly contribute to forming new blood vessles.[21] Additionally, optimization of several factors in the treatment (i.e. at which time point in the disease process to deliver cells, route of administration, cell type etc.) may result in better therapeutic effects.[21] Yet, the observation that variation in these factors in previous studies failed to show a significant therapeutic benefit to treat their target diseases suggests that failure of therapeutic efficacy cannot be fully explained by sub-optimization of such factors. Second, another widely known issue is the low rate of stem cell survival/engraftment *in vivo*. For example, in animal studies, only 20% of the delivered cells could be located near the injection site 24 hours post-implantation.[28,29] In the BOOST trial where MNCs were intravenously injected in myocardial infarction patients, only 3% of the implanted cells could be found after 30 days.[29] Together, the data illustrate disappointingly short-term survival and retention rates of implanted cells in the ischemic milieu, which likely results in poor long-term engraftment and limited therapeutic efficacy as previously reported. These results signify the inadequate, limited nature of direct cell injection for lasting effects and imply the need for better delivery vehicles for successful long-term engraftment of delivered stem cells.

EPCs are not an optimal cell source: EPCs (often derived from peripheral blood and positive for both hematopoietic markers and endothelial lineage markers, i.e. $CD34^+$ and $VEGFR2^+$) represents an ideal cell choice for treating vascular/ischemic diseases in theory. They are traditionally directly isolated from bone marrow or blood and have shown to differentiate into cells of endothelial phenotype and functions.[30] However, EPCs suffer from characteristically rare presence and poor proliferative capacity *ex vivo*, which makes it impossible to obtain sufficient cell mass typically used in commercial medical treatment strategies.[31] Additionally, EPCs suffer from poor long-term survival both *in vitro* and *in vivo.*[32,33] Therefore, in practice, EPCs currently have severe limitations for use in stem cell therapies.

MSCs are a promising candidate cell type for vascular cell therapy: There are several advantages to using mesenchymal stem cells (MSCs). One of the most appealing aspects is that MSCs are accessible even for adult patients as they are cultured from the adherent, non-hematopoietic population of the bone marrow.[34] Thanks to their robust proliferation and survival, a single clinical dose of 10^8 of MSCs could be generated within 7 days from roughly 5 ml of bone marrow.[28] However, the challenge is in successfully converting MSCs into endothelial cells, a process which has not been fully perfected.[34,35] Encouragingly, there are few previous studies that have shown MSCs directly contributing to endothelium, smooth muscle cells and even myocytes in cardiovascular repair *in vivo* at low efficiencies.[34] Thus, a significant part of this work (Chapters 4 and 5) is focused on overcoming the major hurdles of utilizing easily obtained bone marrow MSCs for vascular cell therapy by optimizing non-invasive targeted delivery, survival, endothelial potency and vasculogenesis of delivered MSCs *in vivo*.

2.4 Integrins and Downstream Signaling Pathways for Angiogenesis

Integrins mediate cell-material interactions: Integrins are heterodimeric membrane glycoproteins consisting of non-covalent association between an α unit and a β unit. Integrins are receptors for

extracellular matrix proteins and immunoglobulin superfamily molecules, thus they are heavily involved in cell attachment and cell migration processes. With 18 different α units and 8 β units, 24 heterodimeric integrin clusters can be formed, each recognizing and binding single or multiple ligands.[36] For instance, integrins αvβ3, α5β1, αIIbβ3, αvβ6 and α3β1 bind to arginine-glycine-aspartic acid (**RGD**) sequence present in various ligands, and the peptide sequences flanking RGD can impart ligand selectivity. On the other hand, some integrins, such as α4β1, can bind vascular cell adhesion molecule VCAM-1, and promote cell–cell adhesion.[37]

Ligated integrins activate intracellular signaling pathways: While integrins do not have intrinsic enzymatic/kinase activities to those associated with growth factor receptors, they are capable of activating complex intracellular signaling pathways through focal adhesion formation where integrins cluster with kinases [e.g., protein kinase B (**Akt**), extracellular signal-regulated kinase (**ERK1/2**), focal adhesion kinase (**FAK/PTK2**), p38 mitogen activated protein kinases (**MAPK**) and tyrosine-protein kinase (**SRC**)], adaptor proteins, signaling intermediates, cytoskeletal proteins, and other signaling proteins intracellularly.[38,39] These intracellular signaling activities lead to cell migration/movement and morphological changes by providing traction along ECM proteins, as well as by remodeling the cytoskeleton.

Integrin signaling pathways are crucial in endothelial cell functions and angiogenesis: Several earlier studies revealed the important roles of integrins and their associated intracellular signaling pathways in regulating angiogenesis. For example, overexpression of FAK has shown to promote angiogenesis, while deletion of FAK in endothelial cells resulted in defective vasculature development and hemorrhage with reduced tubulogenesis and proliferation capacity *in vitro*.[40,41] These results indicate FAK as a key regulatory player in angiogenesis and vascular development. MAPK signaling pathways can be activated by both integrins or growth factor receptors, and are actively involved in early cardiac/endothelial development.[42] Given these facts, the heavy involvement of integrins in angiogenesis has led to multiple clinical trials where integrin inhibitors were tested to limit cancer

metastasis/progression by limiting angiogenesis.[43] Therefore, elucidating the integrin signaling pathways that drive the pro-vasculogenic material effect of our injectable gelatin hydrogel would provide an advanced means to control stem cell fate for future clinical applications, and we explore this topic in Chapter 5.

2.5 References

[1] Vogel, G. Science 2015, 349(6252), 1035-1035.

[2] Vogel, G. Science 2016, 351(6273), 546-546.

[3] Gonfiotti, A., Jaus, M. O., Barale, D., Baiguera, S., Comin, C., Lavorini, F& Macchiarini, P. The Lancet 2014, 383(9913), 238-244.

[4] Lim, M. L., Firsova, A. B., Feliu, N., Kuevda, E. V., Jungebluth, P., & Macchiarini, P. In Stem Cells in the Lung 2015, Springer International Publishing, (pp. 289-307).

[5] Crowley, C., Birchall, M., & Seifalian, A. M. Journal of tissue engineering and regenerative medicine 2015, 9(4), 357-367.

[6] Jungebluth, P., & Macchiarini, P. In Difficult Decisions in Thoracic Surgery 2014, Springer London, (pp. 565-575).

[7] Atala, A., Kasper, F. K., & Mikos, A. G. Science translational medicine 2012, 4(160), 160rv12-160rv12.

[8] Rouwkema, J., Rivron, N. C., & van Blitterswijk, C. A. Trends in biotechnology 2008, 26(8), 434-441.

[9] Auger, F. A., Gibot, L., & Lacroix, D. Annual review of biomedical engineering 2013, 15, 177-200.

[10] Jain, R. K., Au, P., Tam, J., Duda, D. G., & Fukumura, D. Nature biotechnology 2005, 23(7), 821-823.

[11] Furth, M. E., Atala, A., & Van Dyke, M. E. Biomaterials 2007, 28(34), 5068-5073.

[12] C. A. Schoener, H. N. Hutson, N. A. Peppas, Polym Int 2012, 61, 874.

[13] S. Cammas, K. Suzuki, C. Sone, Y. Sakurai, K. Kataoka, T. Okano, Journal of Controlled Release 1997, 48, 157.

[14] F. Meng, Z. Zhong, J. Feijen, Biomacromolecules 2009, 10, 197.

[15] S. Gorgieva and V. Kokol, in Biomaterials Applications for Nanomedicine, ed. P. R, InTech, 2011, ch. 2, pp. 17-52.

[16] H. B. Bohidar and A. Gupta, Biomacromolecules, 2005, 6, 1623-1627.

[17] A. K. Lynn, I. V. Yannas and W. Bonfield, Journal of biomedical materials research. Part B, Applied biomaterials, 2004, 71, 343-354.

[18] S. K. Mitra, D. A. Hanson and D. D. Schlaepfer, Nature Reviews Molecular Cell Biology, 2005, 6, 56-68

[19] T.-L. Shen, A. Y.-J. Park, A. Alcaraz, X. Peng, I. Jang, P. Koni, R. A. Flavell, H. Gu and J.-L. Guan, The Journal of cell biology, 2005, 169, 941-952.

[20] M. K. Mamidi, R. Pal, S. Dey, B. J. Bin, Z. Zakaria, M. S. Rao and A. K. Das, Cytotherapy, 2012, 14, 902-916.

[21] R. J. Powell, A. J. Comerota, S. A. Berceli, R. Guzman, T. D. Henry, E. Tzeng, O. Velazquez, W. A. Marston, R. L. Bartel, A. Longcore, T. Stern and S. Watling, Journal of vascular surgery, 2011, 54, 1032-1041.

[22] A. H. Kumar and N. M. Caplice, Arterioscler Thromb Vasc Biol, 2010, 30, 1080-1087.

[23] D. Orlic, J. Kajstura, S. Chimenti, I. Jakoniuk, S. M. Anderson, B. Li, J. Pickel, R. McKay, B. NadalGinard, D. M. Bodine, A. Leri and P. Anversa, Nature, 2001, 410, 701-705.

[24] S. Dimmeler, A. M. Zeiher and M. D. Schneider, J Clin Invest, 2005, 115, 572-583.

[25] L. da Silva Meirelles, A. M. Fontes, D. T. Covas and A. I. Caplan, Cytokine & Growth Factor

Reviews, 2009, 20, 419-427.
[26] K. Moazzami, R. Majdzadeh and S. Nedjat, The Cochrane Library, 2011, DOI: 10.1002/14651858.CD14008347.pub14651852.
[27] M. P. Alfaro and P. P. Young, Cell Transplant, 2012, 21, 1065-1074.
[28] P. P. Young, D. E. Vaughan and A. K. Hatzopoulos, Progress in Cardiovascular Dis, 2007, 49, 421- 429.
[29] J. K. Devin and P. P. Young, Curr Opin Invest Drug, 2008, 9, 983-992.
[30] A. J. Devanesan, K. A. Laughlan, H. R. S. Girn and S. Homer-Vanniasinkam, European Journal of Vascular and Endovascular Surgery, 2009, 38, 475-481.
[31] K. Yamahara and H. Itoh, Therapeutic Advances in Cardiovascular Disease, 2009, 3, 17-27.
[32] M. P. Alfaro, S. Saraswati and P. P. Young, Vitam Horm, 2011, 87, 39-59.
[33] J. Wagner, T. Kean, R. Young, J. E. Dennis and A. I. Caplan, Current Opinion in Biotechnology, 2009, 20, 531-536.
[34] S. Gorgieva and V. Kokol, in Biomaterials Applications for Nanomedicine, ed. P. R, InTech, 2011, ch. 2, pp. 17-52.
[35] H. B. Bohidar and A. Gupta, Biomacromolecules, 2005, 6, 1623-1627.
[36] C. J. Avraamides, B. Garmy-Susini and J. A. Varner, Nature Reviews Cancer, 2008, 8, 604-617.
[37] H. Jin and J. Varner, British Journal of Cancer, 2004, 90, 561-565.
[38] S. K. Mitra, D. A. Hanson and D. D. Schlaepfer, Nature Reviews Molecular Cell Biology, 2005, 6, 56-68. 31.
[39] S. K. Mitra and D. D. Schlaepfer, Current opinion in cell biology, 2006, 18, 516-523. [40] X. Peng, H. Ueda, H. Zhou, T. Stokol, T.-L. Shen, A. Alcaraz, T. Nagy, J.-D. Vassalli and J.-L. Guan, Cardiovascular research, 2004, 64, 421-430.
[41] T.-L. Shen, A. Y.-J. Park, A. Alcaraz, X. Peng, I. Jang, P. Koni, R. A. Flavell, H. Gu and J.-L. Guan, The Journal of cell biology, 2005, 169, 941-952.
[42] K.-M. V. Lai and T. Pawson, Genes & development, 2000, 14, 1132-1145.
[43] C. Ruegg and G. C. Alghisi, in Angiogenesis Inhibition, eds. S. P.M. and S. H.J., Springer, 2010.
[44] http://www.organdonor.gov/about/data.html
[45] Lechler, R.I., Sykes, M., Thomson, A.W. and Turka, L.A., 2005. *Nature medicine*, *11*(6), 605-613.
[46] Watson, C.J.E. and Dark, J.H., 2012.. British journal of anaesthesia, 108(suppl 1), i29-i42.
[47] Martin, J.R., Gupta, M.K., Page, J.M., Yu, F., Davidson, J.M., Guelcher, S.A. and Duvall, C.L., 2014. Biomaterials, 35(12), pp.3766-3776.
[48] Wilson, D.S., Dalmasso, G., Wang, L., Sitaraman, S.V., Merlin, D. and Murthy, N., 2010. Nature materials, 9(11), pp.923-928.
[49] Nathan, A., Nugent, M.A. and Edelman, E.R., 1995. Proceedings of the National Academy of Sciences, 92(18), pp.8130-8134.
[50] Zhang, X., Xie, C., Lin, A.S., Ito, H., Awad, H., Lieberman, J.R., Rubery, P.T., Schwarz, E.M., O'Keefe, R.J. and Guldberg, R.E., 2005. Journal of Bone and Mineral Research, 20(12), pp.2124-2137.
[51] Chen, Y.C., Lin, R.Z., Qi, H., Yang, Y., Bae, H., Melero-Martin, J.M. and Khademhosseini, A., 2012. Advanced functional materials, 22(10), pp.2027-2039.

[52] Salamon, A., Van Vlierberghe, S., Van Nieuwenhove, I., Baudisch, F., Graulus, G.J., Benecke, V., Alberti, K., Neumann, H.G., Rychly, J., Martins, J.C. and Dubruel, P., 2014. Materials, 7(2), pp.1342-1359.

Chapter 3

Aim 1: ROS-cleavable proline oligomer crosslinking of polycaprolactone for pro-angiogenic host response

This chapter is taken from:

Lee, Sue Hyun, et al. "ROS-cleavable proline oligomer crosslinking of polycaprolactone for pro-angiogenic host response." *Journal of Materials Chemistry B* 2.41 (2014): 7109-7113.

Abstract: A reactive oxygen species (ROS)-degradable scaffold is fabricated by crosslinking biocompatible, hydrolytically-degradable poly(ε-caprolactone) (PCL) with a ROS-degradable oligoproline peptide, KP_7K. The ROS-mediated degradability triggers favourable host responses of the scaffold including improved cell infiltration and angiogenesis *in vivo*, indicating its unique advantages for tissue engineering applications.

3.1 Introduction

Recent progress in biomaterial development emphasizes the advanced function that enables target-specific therapeutic delivery through a stimuli-responsive structural change in a spatiotemporally controlled manner. These materials have been designed to activate the advanced functions in response to various physiological parameters, such as pH,[2] temperature,[3] protease activities, and redox balance[4] to target a local pathological event in the body. One such biological stimulus that is drawing keen attention recently is reactive oxygen species (ROS) which include hydroxyl radicals ($OH^{\cdot}$), hydrogen peroxides (H_2O_2), peroxynitrites ($ONOO^-$) and superoxides (O_2^-) among others.[5] While low levels of ROS are part of normal cell metabolism, excessive amounts of

ROS cause oxidative stress and damage critical components of cells at all levels including DNA,[6] proteins,[7] and lipids[8] by oxidation. Moreover, chronically increased levels of ROS are present locally in cancer,[9] atherosclerosis,[10] diabetes,[11] infections,[12] inflammatory diseases,[13] and even in the aging process[14] where ROS levels can be 10- to 100-times the normal levels. For example, in the vicinity of activated macrophages that are prevalent in inflammation and implantation sites, the hydrogen peroxide concentration can reach 10 – 100 μM.[15] Therefore, ROS can be considered as a critical parameter indicating local occurrence or progression of such diseases, and ROS-responsive materials are needed to enable site-specific delivery of therapeutics and imaging agents as they can undergo structural changes (e.g., degradation) and release the payload in response to locally overproduced ROS in vivo.

Starting with polypropylene sulfide (PPS) developed in 2004, ROS-sensitive materials are still relatively new, but have been continuously developed due to the increasing demand for various biomedical applications. While numerous other studies focused on designing synthetic polymers that rapidly respond to ROS in nanoscale delivery formats [16] [17] [18], we investigated a peptide oligomer as a ROS-responsive unit for long-term tissue engineering applications. Previous studies have shown that proteins containing aspartic acid, glutamic acid or proline residues are especially prone to oxidative degradation.[19] ROS-sensitive degradability of proline residues has demonstrated particular promise.[20, 21]

In a previous study, we synthesized proline oligomers as a ROS-cleavable crosslinker and extensively characterized its fabrication and response to ROS in vitro.[22] In particular, oligoproline peptides with 5, 7 or 10 proline residues were tested for ROS-mediated degradation by reacting in 5 mM H_2O_2 with 50 μM Cu(II) at 37 °C. All proline residues were cleaved away after 6 days, confirming relatively slow ROS-mediated degradation, compared to PPS that degrades in several hours in oxidative environments.[16]

Therefore, in the current study, we investigated the potential of using an oligoproline-

crosslinked poly(ε-caprolactone) (PCL)-based scaffold in an in vivo model for long-term tissue engineering applications. PCL was chosen as the base polymer, as it is approved by the Food and Drug Administration (FDA) for biomedical applications such as tissue engineering and drug delivery.[23] Furthermore, PCL is known for slow in vivo degradation over several years by hydrolysis of ester bonds, thereby providing a material format where we can impart faster-acting ROS-degradability to the scaffold. We hypothesized that such ROS-degradability of scaffolds would allow for favorable interactions with host cells in vivo where the initial inflammatory host response would degrade the implanted scaffold by excess ROS production and encourage cell infiltration into the scaffold, leading to improved neovascularization and engraftment within the site of implantation.[24] Towards this end, first we modified and improved the chemistry involved to efficiently crosslink PCL with ROS-degradable oligoproline peptides, and studied their chemical and thermal properties as well as their in vitro ROS-degradability. Finally, we implanted the scaffolds subcutaneously in mice to test our hypothesis for the effect of ROS-degradability of scaffold on host-material interaction with an emphasis on vascularization of the implanted scaffold.

3.2 Materials and Methods

Materials: PCL 70-90K MW, Lithium Diisopropylamide (LDA), tetrahydrofuran (THF), diethyl ether, dichloromethane (DCM), triethylamine (TEA), dimethylformamide (DMF), N-hydroxysuccinimide (NHS), N,N'-dicyclohexylcarbodiimide (DCC), KBr, NaCl, lipopolysaccharide (LPS), RIPA buffer were used as purchased from Sigma-Aldrich. PEG (2000 MW)-dihydrazide was purchased from Laysan Bio, and KP7K peptides were synthesized on PS3 (Protein Technologies).

Synthesis of PCL-CPCL: In a 500 mL round-bottom flask, 5 g of PCL was dissolved in 400 mL anhydrous THF, and 50 mL of 2 M LDA was added dropwise at -78 °C. Then 50 g of dry CO_2 gas was added into the flask while stirring via subliming dry ice for 50 minutes. After the temperature was raised to 0 °C, 20 g of NH_4Cl in 100 mL H_2O was added to the mixture. PCL-CPCL was filtered,

precipitated in cold diethyl ether and dried under vacuum. Chemical composition was determined by ^{1}H-NMR. Molecular weight properties were determined by gel permeation chromatography against PMMA standards (Agilent Technologies) using a Phenogel 10E3A column (Phenomenex Inc.) in THF.

Synthesis of PCL-(NHS)CPCL: 3 g of 70% PCL-30% CPCL and 2.09 g of NHS were dissolved in 30 mL of dry DCM. 3.74 g of DCC dissolved in 9 mL DCM was added drop by drop, and the reaction continued for 8 hours at 0 °C. After filtration through 2 μm Whatman filter paper, PCL-(NHS)CPCL was precipitated in excess of 1:1 mixture of cold ethyl ether and methanol, and dried under vacuum.

Crosslinking of PCL-(NHS)CPCL and Scaffold Fabrication: 0.8 mmol of PCL-(NHS)CPCL was dissolved in 10 mL DCM, and 0.2 mmol of crosslinkers (KP7K or PEG-dihydrazides) dissolved in 10 mL DCM, 5 mL DMF and 500 μL TEA was added drop by drop. The reaction continued for 8 hours in room temp, then precipitated in excess of 1:1 mixture of cold ethyl ether and methanol. After dissolving in 10 mL DCM, the mixture was poured over 10 g of NaCl (sieved to 245 – 410 μm) bed in a 100 mm Teflon dish. After drying overnight in vacuum, scaffolds were punched with a 6 mm punch, NaCl was leached in daily changes of excess H_2O over 4 days.

Fourier Transform Infrared Spectroscopy: 2 mg of polymer scaffold samples and 100 mg of KBr were ground and pressed to form pellets. Samples were subjected to FTIR spectroscopy using a Bruker PMA 50 spectrophotometer. Scanning was conducted from 4000 to 400 cm^{-1} with 64 scans averaged and 4 cm^{-1} resolution.

Swelling Ratio Measurement: Scaffolds were incubated in PBS at 37 °C overnight, and wet masses of the scaffolds were measured. Swollen scaffolds were blotted dry to remove excess buffer before weighing. Swelling ratio was calculated according to the formula: swelling ratio = (wet mass)/(dry mass).

Gel Content Measurement: 5-10 mg scaffolds were washed three times with 3 mL THF. Remaining polymer was dried in vacuum and weighed, and gel content was calculated according to the formula: gel content (%) = (remaining polymer mass after washes)/(dry mass before washes) x 100.

Differential Scanning Calorimetry: All polymeric scaffolds were analyzed for thermal transitions and heat capacity via on a TA Instruments Q2000 DSC. Samples were weighed (2−5 mg) and pressed in aluminum sample pans with tops. The measurement procedure included two temperature sweeps from −50 to 100 °C at a ramp rate of 10 °C/min. The values from the second sweep were reported such that thermal history was erased.

Dynamic Mechanical Analysis: To determine mechanical properties, rectangular strips (~20mm x ~4.0mm x ~0.1mm) were loaded onto a tension clamp and subjected to a stress ramp of 1.0 MPa min^{-1} until break at 37 ^{o}C using a TA Instruments Q2000 dynamic mechanical analyzer (DMA).

Oxidation Experiments: To investigate oxidative degradation, scaffolds were incubated in PBS with or without 1 mM SIN-1 (Invitrogen) for 28 days at 37 °C. Buffers were changed daily owing to the relatively short half-life of SIN-1 in aqueous environments (<10 h). At 30 days post incubation, scaffolds were dried in vacuum.

Cell Studies: For cell studies involving bone marrow-derived macrophages (BMDMs), 4 week old C57/bl6 mice were used. Briefly, after euthanasia, femurs and tibia were collected and flushed with RPMI 1640 media (Invitrogen), and collected cells were plated on non-tissue culture treated plates in RPMI 1640 containing 10% FBS, 1% penicillin-streptomycin, and 20% L929-conditioned DMEM medium for 7 days. On day 7, proper differentiation into BMDM was confirmed via immunostaining against CD11b and F4/80. Cells were directly seeded onto scaffolds in 24-well plate at a density of 300,000 cells/cm^2, and cultured with or without 50 μg LPS for inflammatory activation with ROS overproduction for 7 days. Cells were removed by washing the scaffolds with RIPA buffer and H_2O.

Scanning Electron Microscopy: SEM was performed on a Hitachi S-4200 system. An accelerating voltage of 2.5 kV was used for all images. To prepare scaffolds for imaging, scaffolds were sputter-coated with gold (Cressington Sputter Coater 1080) at a plasma current of 30 mA for 120 s.

Subcutaneous Implantation: All animal work and related protocols were approved and performed in accordance with Vanderbilt IACUC. Wild type C57/bl6 mice were anesthetized with 1.5 L/min oxygen

and 1.5% isoflurane on a warm water blanket, and shaved. A small 1.5 cm longitudinal incision was made on the ventral side, and scaffolds were inserted into individual subcutaneous pockets. The skin incision was closed with sutures.

H&E Staining and Cell infiltration Analysis: Scaffolds were collected and fixed in 4% paraformaldehyde overnight, and embedded in OCT compound (TissueTek) for cryosectioning. Sections were then submitted to Vanderbilt Translational Pathology Shared Resources Core for H&E staining. Brightfield microscope images were acquired using a Nikon Eclipse Ti microscope (Nikon, Japan), and color deconvolution plugin in ImageJ (National Institutes of Health, USA) was used for quantifying the density of nuclei in tissue/scaffold sections.

Perfusion and Microangiography: At 2 weeks post implantation, mice were perfused under heavy, near-lethal level of anesthesia with 4% isoflurane in 2 L/min oxygen. First, PBS containing 0.1 mg/ml heparin sulfate was injected into the left ventricle to exsanguinate via the cut inferior vena cava. Then mice were perfused with PBS containing fluorescent microbeads (Invitrogen) for micro-angiography. Micro-angiograms were then acquired using a Zeiss 710 confocal laser microscope. ImageJ (National Institutes of Health, USA) was used for all image preparation and analysis, including z-stacking fluorescence images.

Gene Expression Analysis via Quantitative Polymerase Chain Reaction (qRT-PCR): Samples were homogenized in Trizol (Invitrogen), and RNA was collected using RNeasy kit (Qiagen). RNA concentration and 260/280 ratios were measured on a TECAN M1000 plate reader. RNA was treated with DNAse to eliminate genomic contamination, and reverse-transcribed using High Capacity cDNA Synthesis Kit (ABiosystems). SYBR Green PCR mix (Biorad) was used for quantitative PCR. Each sample containing at least 40 ng cDNA and 500 nM of each primer with annealing temperature at 55°C was run in technical triplicates, followed by melting curve analysis. Raw data were analyzed using CFX Manager (Biorad), and biological replicates from different animals were combined. GAPDH expression was used as a reference gene, where the GAPDH expression level divides each

gene expression level for normalization. This relative gene expression to GAPDH is then normalized to that of the control PCL condition. Primers used in this study include: GAPDH primers 5' TGAAGCAGGCATCTGAGGG 3' and 5'CGAAGGTGGAAGAGTGGGAG 3', CD31 primers 5' TCCCTGGGAGGTCG TCCAT 3' and 5' GAACAAGGCAGCGGGGTTTA 3', and VEGFA 5' ATGCGGATCAAACCTCACCA 3' and 5' CCGCTCTGAACAAGGCTCAC 3'.

Statistical Analysis: Results are presented as means ± standard deviation (SD) or standard error mean (SEM) as indicated. Comparisons among different conditions were performed via ANOVA, followed by Tukey's HSD test in Prism 6 (Graphpad). For all statistics, $p < 0.05$ was considered statistically significant, and such significance is indicated where appropriate.

3.3 Results and Discussion

To incorporate crosslinkers, PCL was functionalized with carboxyl groups (Figure 3.1A).[25] The ratio of the integral peaks for carboxylated PCL (CPCL) (3.4 and 9.2 ppm) and unmodified PCL (4.1 ppm) from the ^{1}H-NMR spectrum revealed a molar composition of 70% PCL-30% CPCL. Of note, the extent of carboxylation can be varied from 5 - 60% by varying the duration of the reaction (data not shown). The molecular weight of 70% PCL-30% CPCL (number-average molecular weight (M_n) = 95.5 kDa; polydispersity (PDI = M_w/M_n) of 1.40) is comparable to the unmodified starting material,

Figure 3.1 (A) Synthesis and fabrication of porous KP_7K or PEG-crosslinked 70%PCL-30%CPCL scaffolds with a representative SEM image. **(B)** ROS-cleavable peptide KP_7K [1] and PEG-dihydrazide (control) crosslinkers.

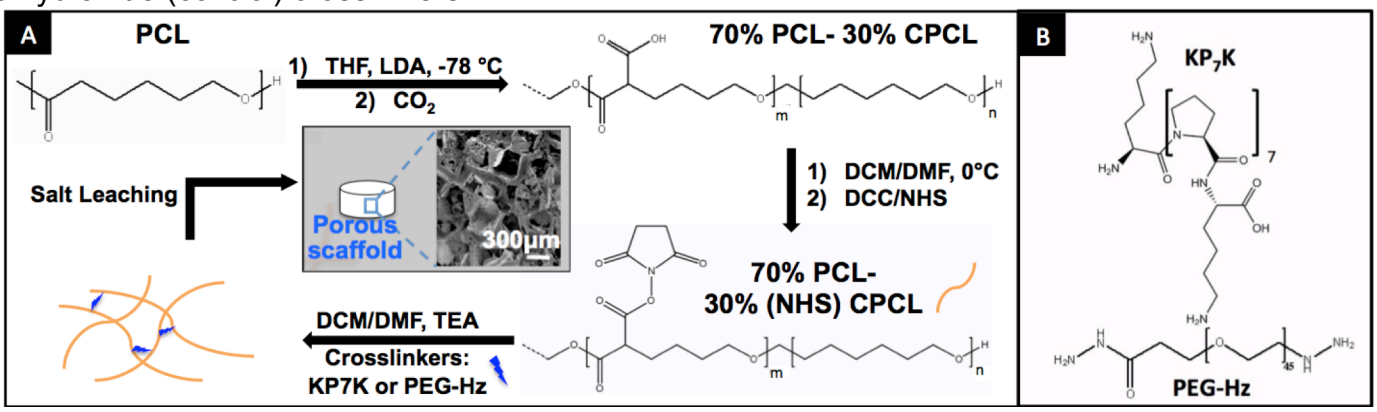

100%PCL (M_n = 87.0 kDa; PDI = 1.28), indicating no significant hydrolysis of polyester chains during the reaction with LDA. Figure 3.1B shows the ROS-cleavable KP_7K peptide crosslinker and poly(ethylene glycol) (PEG)-dihydrazide crosslinker used as a control in this study. Dicyclohexylcarbodiimide (DCC)/N-hydroxy-succinimide ester (NHS) was used to crosslink 70% PCL-30% CPCL with the crosslinkers. Rapid crosslinking was observed as the mixture began gelling immediately.

We then verified and characterized the crosslinking. Successful crosslinking was first confirmed by FTIR, where amide (I) C=O band at ~1620 cm^{-1} was observed for both PEG-dihydrazide and KP_7K-crosslinked 70% PCL-30% CPCL, as well as increased absorbance for N-H stretching and O-H stretching from water molecules around 3200~3700 cm^{-1} (Figure 3.2A).[26] Next, gel content measurement further characterized the degree of crosslinking, where PEG-dihydrazide and KP_7K-crosslinked scaffolds exhibited 73 ± 7.1% and 82 ± 5.9% in gel contents with THF washes, respectively, indicating a high degree of crosslinking within these scaffolds.

Crosslinking of 70% PCL-30% CPCL with hydrophilic KP_7K peptide crosslinkers altered physicochemical properties of the scaffolds, as evidenced by the changes in the swelling ratios of the scaffolds. When incubated in PBS at 37 °C for 1 day, uncrosslinked 30% CPCL-70% PCL had

Figure 3.2. Characterization of scaffolds. **(A)** FTIR spec for 70%PCL-30%CPCL crosslinked with either KP_7K (KP_7K X) or PEG-Hz (PEG X). (B) Swelling ratios of porous scaffolds. Error bar= ±1 SD. **(C)** Thermal characterization of porous scaffolds by DSC.

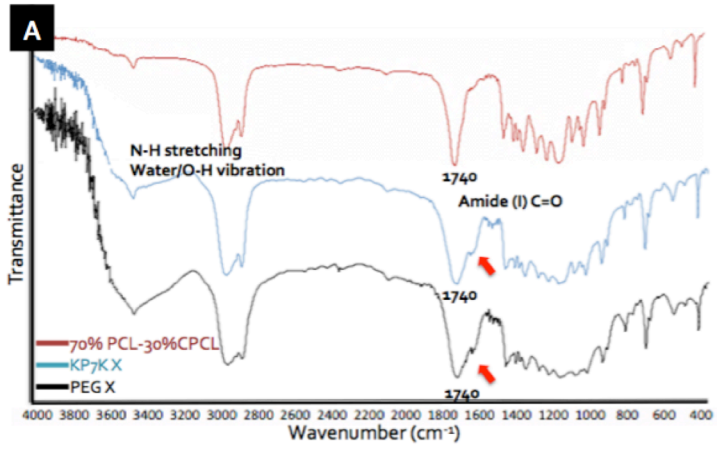

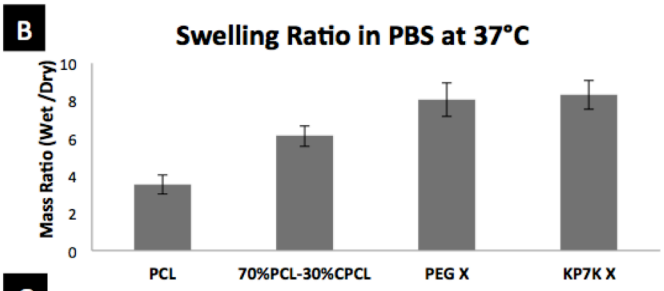

C

	Tc (C°)	ΔHc (J*g-1*C°-1)	Tm (C°)	ΔHf (J*g-1*C°-1)
PCL	28.9	73.1	55.1	71.7
70%PCL-30%CPCL	29.7	60.1	55.3	52.5
PEG X	10.2	37.4	43.1	33.9
KP7K X	14.0	34.6	42.5	33.0

significantly increased the swelling ratio compared to original PCL, and the highly hydrophilic nature of both crosslinkers further increased the swelling ratios of the crosslinked scaffolds (Figure 3.2B). Such increases in hydrophilicity are desirable as it may improve cell attachment and infiltration compared to hydrophobic 100% PCL *in vivo*. [27]

Similarly, the series of modifications made on PCL significantly altered the thermal properties (Figure 3.2C). First, carboxylation of PCL resulted in reduced heats of crystallization (ΔH_c) and melting (ΔH_f), as the carboxyl groups disrupted the packing of semi-crystalline PCL chains to some degree and resulted in less crystallinity. Then, the crosslinking of KP_7K or PEG-dihydrzide with 70% PCL-30% CPCL further disrupted the crystallinity of PCL and reduced the polymer chain flexibility, resulting in drastic decreases in temperatures of crystallization (T_c) and melting (T_m), as well as in ΔH_c and ΔH_f.[28] These changes in the thermal properties resulting from carboxylation and crosslinking can significantly influence material properties, which was exhibited in elastic modulus measured by dynamic mechanical analysis (DMA). Non-porous, thin films were prepared and measured for their elastic moduli in wet conditions at 37 °C. While PCL and 70% PCL-30% CPCL were similar at 77.0 ± 6.0 MPa and 82.5 ± 4.7 MPa, respectively, both PEG- and KP7K- crosslinked conditions exhibited significantly reduced elastic moduli at 22.7 ± 2.7 MPa and 46.4 ± 0.4 MPa (each condition with N=3). The drastic decreases in elastic moduli in the crosslinked conditions are congruent with the decreases in crystallinity (T_c and ΔH_c), caused by crosslinking. Thus, we have shown and proven the effects of crosslinking on PCL in several aspects.

The ROS-degradability of KP_7K-crosslinked scaffold was demonstrated by changes in thermal properties (Fig. 3.3A). Scaffolds were incubated in PBS at 37 °C with or without daily changes of 1 mM SIN-1 for 30 days which degrades into superoxides and nitric oxides to form peroxynitrites. [29] Most notably, the T_c value of the KP_7K-crosslinked scaffold increased significantly with SIN-1 treatment compared to the ones of day 0 and PBS only condition on day 30, as radicals produced from SIN-1 degraded KP_7K crosslinkers, and the newly freed polymer chains likely underwent

Figure 3.3. Characterization of scaffold degradation in response to ROS *in vitro*. **(A)** T_c values of scaffolds obtained from DSC after daily changes of PBS with or without 1mM SIN-1 over 30 days at 37°C. **(B)** SEM images of the scaffold surface after culturing mouse bone marrow-derived macrophages (BMDMs) for 7 days with or without LPS stimulation. **(C)** Quantification of pores created by BMDMs on KP_7K-crosslinked scaffold surface on day 7.

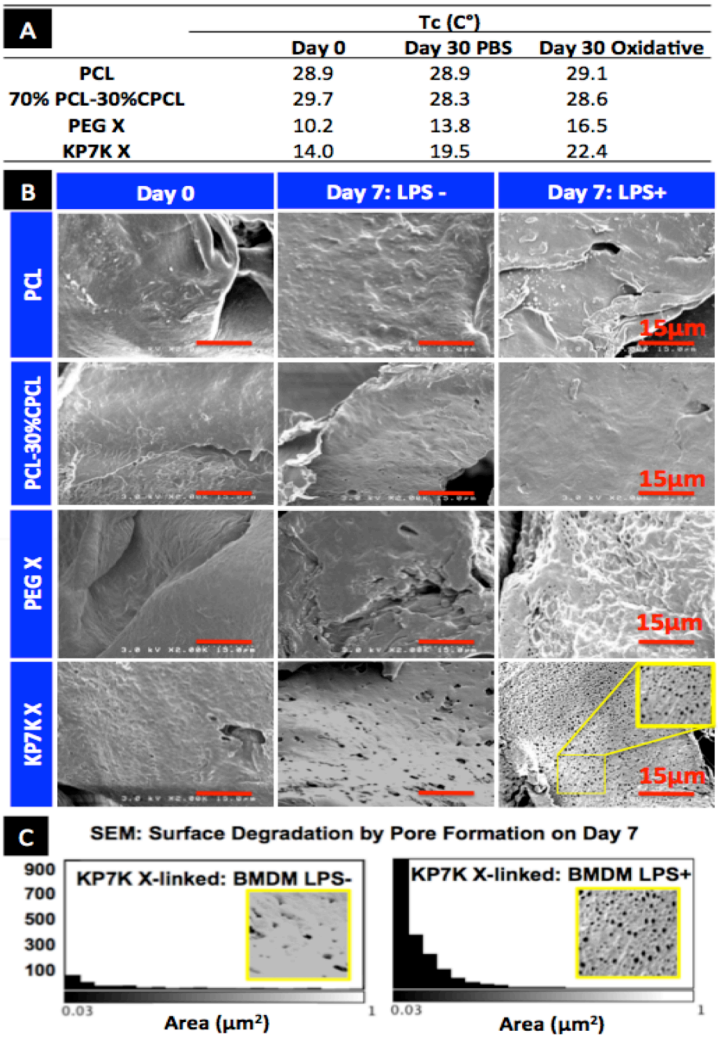

reorganization and recrystallization.[28] In contrast, the uncrosslinked PCL and 70% PCL-30% CPCL scaffolds showed minimal changes in the T_c. PEG-crosslinked scaffolds also degraded with SIN-1 treatment, albeit to a lesser degree than the KP_7K-crosslinked scaffolds. Interestingly, Reid et al. has shown that PEG also degrades in response to ROS produced from Fenton reaction with 50% (w/v) H_2O_2 and 6.2 mM $FeCl_3$ or from radicals produced by UV degradation of 30% H_2O_2.[30] However, PEG and PEG-crosslinked scaffolds might require supraphysiological levels of ROS for degradation which may not be biologically relevant.

The degradation of KP_7K scaffold was accelerated in a physiologically relevant ROS environment *in vitro* where mouse bone marrow-derived macrophages were seeded on the scaffolds with or without the stimulation with 50 μg/ml LPS (Figure 3.3B-C).[31] As an endotoxin, LPS activates macrophages to overproduce ROS and reactive nitrogen species (RNS) including nitric oxide (NO), nitrite (NO_2^-) and peroxynitrite ($ONOO^-$).[32] After removing cells and protein debris from the scaffold, the scaffold surface was imaged by scanning electron microscopy (SEM) (Figure 3.3B). ROS-cleavable KP_7K-crosslinked scaffolds evidently formed numerous pores < 1 um^2, especially when seeded with LPS activated BMDMs, while PEG-crosslinked scaffolds appeared to maintain their smooth surface over 7 day culture. Quantification of this pore formation after 7 day culture (Figure 3.3C) reveals that sub-micron diameter pores increased by more than 10-folds for KP_7K-crosslinked scaffolds cultured with LPS-activated BMDMs, whereas when cultured without LPS, the pore generation was minimal. These results prove that KP_7K-crosslinked scaffolds degrade in response to the physiological levels of ROS produced by activated BMDMs.

While PCL is known to slowly undergo hydrolytic chain scission over several years and become 6-hydroxylcaproic acid that is safely removed from the body,[33] we expected that the initial host immune response to implants would degrade ROS-degradable KP_7K into α-aminobutyric acids that can be used for biosynthesis, while leaving PEG crosslinkers intact due to its non-biodegradability.[34] Therefore, we tested our hypothesis that ROS-degradability of the scaffolds would encourage cell infiltration in a host-responsive manner, thereby improving vascularization of the constructs *in vivo* (Figure 3.4). Scaffolds were subcutaneously implanted in mice for 2 weeks, and sections were stained with H&E to determine host cell infiltration (Figure 3.4A). While cell infiltration is observed in all the constructs, there are some noticeable differences between the materials. When the density of nuclei is determined per tissue/scaffold area from H&E stained sections (Figure 3.4B), it is evident that PCL-30% CPCL had significantly less cells infiltrating compared to PCL, possibly due to the negative charges on carboxyl groups. PEG-crosslinked scaffolds showed a similar amount of

Figure 3.4. (A) After 2-week subcutaneous implantation, scaffolds were stained with H&E (purple: cytoplasm, dark blue: nuclei; scale bar = 50 μm), and imaged for angiography (scale bar = 300 μm). **(B)** Cell infiltration was quantified by Area (nuclei) / Area (tissue) (%) from H&E stained sections. **(C)** mRNA expression of angiogenesis markers by qRT-PCR (N=4; Error = ±1 SEM).

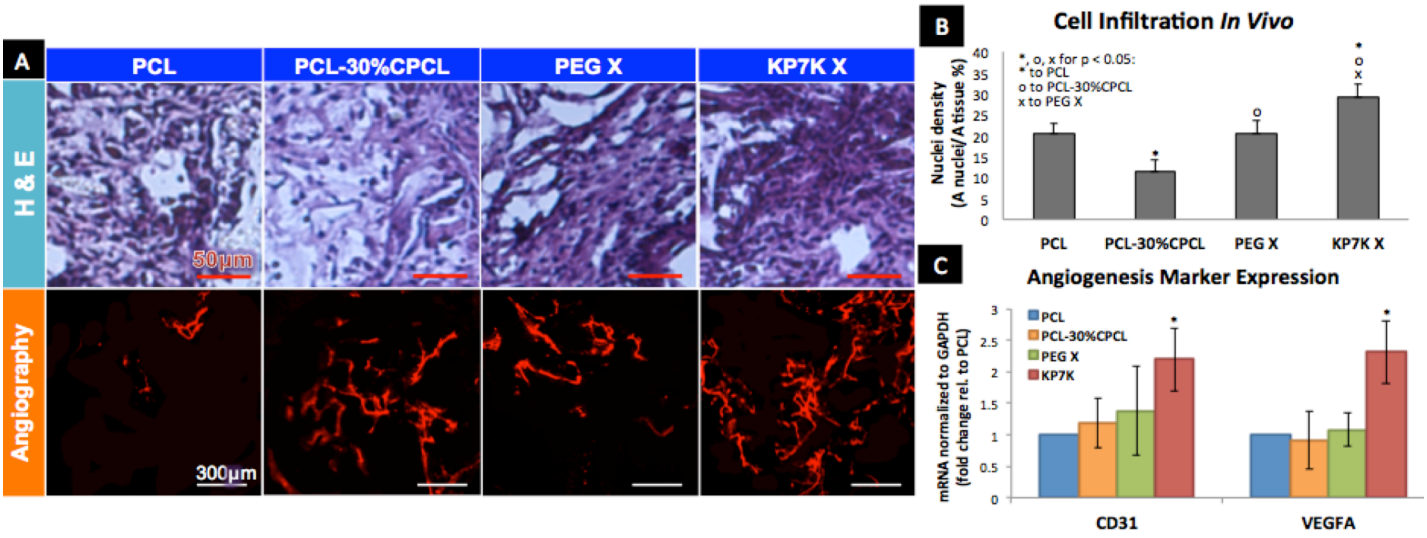

infiltrating host cells compared to PCL, and more importantly, KP_7K-crosslinked scaffolds exhibited the highest nuclei density with 50% more cells infiltrating compared to PCL. Additionally, mice were perfused through the heart with fluorescent microbeads for angiography before harvesting[35] (Figure 3.4A), and the implanted scaffolds were collected for gene expression analysis (Figure 3.4C). While PCL-30% CPCL and PEG-crosslinked scaffolds showed similar levels of neovasculature formation compared to PCL, KP_7K-crosslinked scaffolds significantly promoted angiogenesis, as evidenced by abundant functional, perfusable blood vessels shown in the angiograms, compared to those of PCL scaffolds. This result was further supported by significant increases in gene expression of angiogenesis markers (CD31 and VEGFA)[36] assessed by quantitative RT-PCR (Figure 3.4C), indicating that crosslinking with KP_7K significantly increases blood vessel growth into the scaffolds upon implantation. This is likely due to the fact that early inflammatory responses resulted in degradation of KP_7K-crosslinked scaffolds, which enhances cell infiltration and growth of host cells into the implanted scaffolds, thereby promoting angiogenesis, compared to other conditions that degrade slowly through hydrolysis only. It is also possible that the oligoproline peptides themselves

may have collagen-mimetic functions and properties, as oligoproline peptides mimic collagen in both chemical composition and structure[37]. However, further studies are required to confirm this possibility.

This study demonstrated synthesis and crosslinking of 70% PCL-30% CPCL with ROS-cleavable KP_7K and PEG-dihydrazide crosslinkers via DCC/NHS coupling. To examine their ROS-mediated degradation in a physiologically relevant condition, BMDMs were cultured on the scaffolds under LPS treatment to stimulate their ROS overproduction *in vitro*. The KP_7K-crosslinked scaffolds underwent significant surface degradation in response to overproduced ROS from activated BMDMs. Furthermore, angiogenesis was significantly promoted within the implanted KP_7K-crosslinked scaffolds. This pro-angiogenic behavior can likely be explained by ROS production from host inflammatory cells which induce scaffold degradation and pore generation, resulting in enhanced host cell infiltration into the scaffolds. We have shown that KP_7K-crosslinked 70%PCL-30%CPCL is 1) degradable in response to physiologically relevant ROS levels which allows for better host cell infiltration, and 2) pro-angiogenic *in vivo* via host-material interactions.

While various stimuli-sensitive materials have been developed in nano- to microscale formats as drug delivery vehicles, applying large-scale stimuli-sensitive scaffolds for tissue engineering remain underexplored. Here, we demonstrated the unique advantages of applying ROS-responsive scaffolds in improving vascularization, which is currently an unmet need in the field of tissue engineering. Further studies are required to understand the mechanism by which ROS-degradable KP_7K-crosslinked scaffolds promote angiogenesis with favorable host response. In this way, the scaffold design can be improved to achieve successful engraftment and better clinical outcomes in the future.

3.4 References

1. S. S. Yu, R. L. Koblin, A. L. Zachman, D. S. Perrien, L. H. Hofmeister, T. D. Giorgio and H.-J. Sung, *Biomacromolecules*, 2011, 12, 4357-4366.
2. C. A. Schoener, H. N. Hutson and N. A. Peppas, *Polym Int*, 2012, 61, 874-879.
3. S. Cammas, K. Suzuki, C. Sone, Y. Sakurai, K. Kataoka and T. Okano, *Journal of Controlled Release*, 1997, 48, 157-164.
4. F. Meng, Z. Zhong and J. Feijen, *Biomacromolecules*, 2009, 10, 197-209.
5. S. Papa and V. P. Skulachev, *Molecular and cellular biochemistry*, 1997, 174, 305-319.
6. H. Wiseman and B. Halliwell, *Journal of biochemistry*, 1996, 313, 17-29.
7. R. T. Dean, S. Fu, R. Stocker and M. J. Davies, *The Biochemical journal*, 1997, 324 (Pt 1, 1-18.
8. R. J. Aitken, J. S. Clarkson and S. Fishel, *Biology of reproduction*, 1989, 41, 183-197.
9. L. Vaccari, D. Canton, N. Zaffaroni, R. Villa, M. Tormen and E. di Fabrizio, *Microelectronic Engineering*, 2006, 83, 1598-1601.
10. K. Sugamura and J. F. Keaney, *Free Radical Biology & Medicine*, 2011, 51, 978-992.
11. N. Houstis, E. D. Rosen and E. S. Lander, *Nature*, 2006, 440, 944-948.
12. E. Rastew, J. B. Vicente and U. Singh, *Int J Parasitol*, 2012, 42, 1007-1015.
13. I. Rahman, *J Biochem Mol Biol*, 2003, 36, 95-109.
14. L. V. Papp, J. Lu, A. Holmgren and K. K. Khanna, *Antioxidants & redox signaling*, 2007, 9, 775-806.
15. W. Droge, *Physiol. Rev.*, 2002, 82, 47-95.
16. A. Napoli, M. Valentini, N. Tirelli, M. Muller and J. A. Hubbell, *Nature materials*, 2004, 3, 183-189.
17. D. Wilson, G. Dalmasso, L. Wang, S. Sitaraman, D. Merlin and N. Murthy, *Nautre Materials*, 2010, 9, 923-928.
18. S. H. Lee, M. K. Gupta, J. B. Bang, H. Bae and H.-J. Sung, *Advanced Healthcare Materials*, 2013, 2, 908-915.
19. E. R. Stadtman and R. L. Levine, *Amino acids*, 2003, 25, 207-218.
20. W. M. Garrison, *Chem . Rev*, 1987, 87, 381-398.
21. a. Amici, R. L. Levine, L. Tsai and E. R. Stadtman, *The Journal of biological chemistry*, 1989, 264, 3341-3346.
22. S. S. Yu, R. L. Koblin, A. L. Zachman, D. S. Perrien, L. H. Hofmeister, T. D. Giorgio and H.-J. Sung, *Biomacromolecules*, 2011, 12, 4357-4366.
23. C. X. Lam, D. W. Hutmacher, J. T. Schantz, M. A. Woodruff and S. H. Teoh, *Journal of biomedical materials research. Part A*, 2009, 90, 906-919.
24. H. J. Sung, C. Meredith, C. Johnson and Z. S. Galis, *Biomaterials*, 2004, 25, 5735-5742.
25. M. K. Gupta, J. M. Walthall, R. Venkataraman, S. W. Crowder, D. K. Jung, S. S. Yu, T. K. Feaster, X. Wang, T. D. Giorgio, C. C. Hong, F. J. Baudenbacher, A. K. Hatzopoulos and H. J. Sung, *PloS one*, 2011, 6, e28935.
26. Z. Movasaghi, S. Rehman and D. I. ur Rehman, *Applied Spectroscopy Reviews*, 2008, 43, 134-179.
27. Z. Ma, Z. Mao and C. Gao, *Colloids and surfaces. B, Biointerfaces*, 2007, 60, 137-157.
28. L. Mandelkern, *Chem. Rev*, 1995, 56, 903-958.

29. N. Hogg, V. Darley-Usmar, M. WIlson and S. Mocada, *Biochem. J*, 1992, 281, 419-424.
30. B. Reid, M. Gibson, A. Singh, J. Taube, C. Furlong, M. Murcia and J. Elisseeff, *Journal of tissue engineering and regenerative medicine*, 2013, DOI: 10.1002/term.1688.
31. J. Weischenfeldt and B. Porse, *CSH protocols*, 2008, 2008, pdb prot5080.
32. C. Amatore, S. Arbault, C. Bouton, J. C. Drapier, H. Ghandour and A. C. Koh, *Chembiochem : a European journal of chemical biology*, 2008, 9, 1472-1480.
33. M. A. Woodruff and D. W. Hutmacher, *Progress in Polymer Science*, 2010, 35, 1217-1256.
34. K. Knop, R. Hoogenboom, D. Fischer and U. S. Schubertf, *Angew. Chem. Int. Ed.*, 2010, 49, 6288-6308.
35. A. L. Zachman, S. W. Crowder, O. Ortiz, K. J. Zienkiewicz, C. M. Bronikowski, S. S. Yu, T. D. Giorgio, S. A. Guelcher, J. Kohn and H. J. Sung, *Tissue engineering. Part A*, 2013, 19, 437-447.
36. T. C. Mineo, *Journal of Clinical Pathology*, 2004, 57, 591-597.
37. S. Gorgieva and V. Kokol, *2. Collagen- vs. Gelatin*, inTech, 2011.

Chapter 4

Aim 2: In Situ Crosslinkable Gelatin Hydrogels for Vasculogenic Induction and Delivery of Mesenchymal Stem Cells

This chapter is taken from:

Lee, Sue Hyun, et al. "In situ crosslinkable gelatin hydrogels for vasculogenic induction and delivery of mesenchymal stem cells." *Advanced functional materials* 24.43 (2014): 6771-6781.

Abstract: Clinical trials utilizing mesenchymal stem cells (MSCs) for severe vascular diseases have highlighted the need to effectively engraft cells and promote pro-angiogenic activity. A functional material accomplishing these two goals is an ideal solution as spatiotemporal and batch-to-batch variability in classical therapeutic delivery can be minimized, and tissue regeneration would begin rapidly at the implantation site. Gelatin may serve as a promising biomaterial due to its excellent biocompatibility, biodegradability, and non-immuno/antigenicity. However, the dissolution of gelatin at body temperature and quick enzymatic degradation in vivo have limited its use thus far. To overcome these challenges, an injectable, in situ crosslinkable gelatin was developed by conjugating enzymatically-crosslinkable hydroxyphenyl propionic acid (GHPA). When MSCs are cultured in 3D in vitro or injected in vivo in GHPA, spontaneous endothelial differentiation occurs, as evidenced by marked increases in endothlelial cell marker expressions (Flk1, Tie2, ANGPT1, vWF) in addition to forming an extensive perfusable vascular network after 2-week subcutaneous implantation. Additionally, favorable host macrophage response is achieved with GHPA as shown by decreased iNOS and increased MRC1 expression. These results indicate GHPA as a promising soluble factor-free cell delivery template which induces endothelial differentiation of MSCs with robust

neovasculature formation and favorable host response.

4.1 Introduction

Numerous material platforms have been funcionalized with biological molecules (e.g. vascular endothelial growth factor) to stimulate a pro-angiogenic response of embedded cells in order to effectively engineer functional new tissue.[1-3] In many of these studies, the pro-angiogenic activity is thought to rely exclusively on the biological molecules that are engrafted or delivered within these constructs, and the direct influence of the material itself has received little attention. Although these approaches have shown promise in vascularizing engineered constructs, they face significant challenges for stem cell delivery, because encapsulated stem cells show limited survival, vascular diffferentiation, and functional regeneration that are required for effective repair of vascular tissue.[4] Moreover, variations in the spatiotemporal release, batch-to-batch uniformity, and efficiency of presentation of biological molecules has hindered progress since these problems could result in heterogenous differentiation with unexpected side effects. Therefore, the principles for designing functional materials as a instructive cell delivery platform are evolving. While the traditional view considered the extracellular matrix (ECM) as a passive scaffold material mainly providing biomechanical support, it is now clear that ECM plays a central role in the outside-in signaling that influences the structure and functions of the cells with which it interacts.[5-7] Therefore, engineered ECM without the addition of extrinsic bioactive molecules represents an ideal functional material source that (1) can be specifically modified to engraft stem cells for maximal cell survival; (2) provide uniform functional and structural cues to cells in order to minimize spatiotemporal variations; and (3) instruct tissue regeneration as an all-in-one directive material platform that does not require release or presentation of additional biological molecules.

Mesenchymal stem cells (MSCs) are generated in culture from the adherent, non-hematopoietic population of the bone marrow (BM).[8] Due to their robust proliferation and survival, a

single clinically-relevant dose (~10^8) of therapeutic-grade MSCs can be obtained in 7 days from only a small starting volume (5 ml) of BM.[9] However, MSCs face the challenge of poor engraftment when delivered in vivo.[8,10] Moreover, the potential of MSCs to differentiate into endothelial cells has not been fully harnessed and remains unclear.[8,11] Published reports suggest that MSCs can contribute to endothelium, smooth muscle, or even myogenic tissue in cardiovascular repair at low levels; however, heterogeneous cellular responses have blurred the understanding of this process.[11, 12] Furthermore, clinical delivery of MSCs to diseased vascular tissue has proven unsuccessful, due primarily to ineffective retention of the cells at the site of implant, suggesting that an optimized, biocompatible delivery system for MSCs would be highly valuable. There have been several reports studying methods to differentiate MSCs into endothelial cells.[13-16] However, most studies employed in vitro experiments, thus would require pre-differentiation of MSCs prior to transplantation. Additionally, none of these approaches enables dynamic, in situ endothelial differentiation upon engraftment to a target site. Hence, a functional material that not only provides the mechanical support for the implanted stem cells but also serves as a guide for in situ stem cell differentiation while maintaining cell viability is highly desirable, but largely lacking to this date.

Gelatin, a form of denatured collagen, can be an ideal material source as it is known for its excellent biocompatibility and biodegradability, as well as adhesiveness for cell attachment, and absence of immuno/antigenicity.[17] However, the in vivo application of gelatin has been limited thus far due to its low upper critical solution temperature and quick enzymatic degradation, resulting in few experiments that have aimed to understand the functional impact of gelatin for stem cell delivery.[18] To address these issues, we have recently developed injectable, in situ-crosslinkable gelatin hydrogels.[19] Conjugation of hydroxyphenyl propionic acid to the free amines of gelatin (GHPA) enabled rapid H_2O_2- and horseradish peroxide (HRP)-mediated crosslinking. Such modification allowed the use of gelatin as an injectable thermostable hydrogel with tunable degradation resistance and mechanical properties for in vivo applications.

When encapsulated and cultured within GHPA hydrogels, MSCs showed high cell viability at 15 days with de novo expression of endothelial-specific markers in vitro, and formed perfusable vascular networks that resulted from MSCs undergoing endothelial differentiation in vivo. Our study indicates that GHPA hydrogels are an ideal platform for regenerating vascularized tissue from encapsulated MSCs in vivo, and display intrinsic properties that stimulate vascular induction. The GHPA hydrogels can be combined with established stem cell therapies to develop the next generation of clinically-applicable materials for treating severe vascular diseases and damage.

4.2 Experimental Section

Materials: Gelatin (type A from porcine skin, >300 Bloom), 3-(4-hydroxyphenyl) propionic acid (HPA), 1-ethyl-3-(3-dimethylaminopropyl)-carbodiimide (EDC), N-hydroxy-succinimide (NHS), peroxidase from horseradish (HRP type VI, 250–330U/mg solid), hydrogen peroxide (H_2O_2) were obtained from Sigma Aldrich (St. Louis, MO, USA). Dimethylformamide (DMF) was obtained from Junsei (Tokyo, Japan). Dulbecco's modified Eagle medium (DMEM), penicillin–streptomycin (P/S), fetal bovine serum (FBS), Dulbecco's phosphate buffered saline (DPBS) and trypsin–EDTA were purchased from Gibco BRL (Grand Island, NY, USA). All chemicals and solvents were used as received.

Synthesis and chemical characterization of Gelatin-Hydroxyphenyl Propionic Acid (GHPA): Synthesis of GHPA has been described previously.[19] Briefly, hydroxyphenyl propionic acid (HPA) was first activated with 1-ethyl-3-(3-dimethylaminopropyl)-carbodiimide (EDC), N-hydroxysuccinimide (NHS) in a co-solvent of water and DMF (volume ratio of 3: 2). The activated HPA solution was then added to the pre-heated gelatin solution and stirred at 40°C for 24 hours. The resulting solution was transferred into a dialysis bag (MWCO. 3.5 kDa), dialyzed against deionized water for 3 days, filtered, and lyophilized to obtain the GHPA conjugates (Figure 1A). GHPA was characterized by ^{1}H NMR spectroscopy (AS400, OXFORD instruments, UK), and the phenolic contents of the conjugates were

measured quantitatively at 275 nm using a UV visiblespectrophotometer (V-750 UV/vis/NIR, Jasco, Japan).

Characterization of Elastic/Storage Moduli (G') of GHPA: GHPA was dissolved in DMEM media at 3-7% (wt) and divided into two aliquots; one was mixed with horseradish peroxidase (HRP) at the final concentration of 2.5μg/ml, while the other aliquot was mixed with H_2O_2 at the final concentrations of 0.0025-0.01% (w/v). Solutions were loaded onto separate syringes, and a dual-syringe applicator were used to evenly eject the two solutions, ensuring proper mixing and gelling (Figure 1B). Storage moduli (G') was measured in a parallel plate setting on a TA Instrument RA2000 rheometer in oscillation mode with a frequency of 1 Hz and 0.1% strain at 37°C.

In Vitro 3D Culture of MSC in GHPA Gels: Wild type murine mesenchymal stem cells (MSCs, GIBCO) or Flk1-LacZ transgenic murine MSCs were used (Jackson Laboratories). GHPA and H_2O_2 were dissolved in DMEM media at various % (w/v) as indicated, while a constant concentration of 2.5 μg/ml HRP was used in all conditions. Cells were added to the GHPA+HRP solution at the final concentration of 10^6 cells/ml. The same number of cells was seeded on tissue culture plate without GHPA gel to serve as a control. After GHPA gelled on the well plate, DMEM supplemented with 10% FBS and 1% penicillin-streptomycin was added and media was changed every day over 15 days.

Cell Viability Assay: Cell viability was measured at days 1, 7, and 15 post culture using 5μM resazurin (Sigma). After 4 hours incubation of resazurin with cells, test culture media were transferred to a new 96-well plate for fluorescence readout at 590 nm using a plate reader (M1000, Tecan, Mannedorf, Switzerland). On the same days, cells were also incubated in media containing 1μM calcein AM (Invitrogen) and 1μg/ml propidium iodide (Sigma) for 15 minutes and then imaged by a Zeiss 710 confocal laser scanning microscope for identification of live/dead cells.

MSC Delivery in GHPA Gels on Polyvinyl Alcohol (PVA) Scaffolds In Vivo: All animal procedures were approved and performed in accordance with Vanderbilt Institutional Animal Care and Use Committee. With heterozygous Flk1-LacZ transgenic murine MSCs whose Flk1 was partially replaced

by promoter-less LacZ, Flk1+ cells can then be detected by beta-galactosidase staining. GHPA and H_2O_2 were dissolved in DMEM media at various % (w/v) as described above, while a constant concentration of 2.5μg/ml HRP was used in all conditions. Flk1-LacZ MSC ($5x10^5$)-containing GHPA gel solutions in a total volume of 60 μl were loaded on porous 6 mm-diameter PVA scaffolds (Medtronics). As a control, porous PVA scaffolds loaded with non-crosslinked GHPA + HRP gel solution containing Flk1-LacZ MSCs were implanted. The gel-scaffold complexes were then subcutaneously implanted aseptically on the ventral side of 5-month-old female C57/bl6 mice (Jackson Lab) for 2 weeks, and the procedure was previously described (Figure 5A).[40] Briefly, mice were anesthesized with 1.5 L/min oxygen and 1.5% isoflurane on a warm water blanket, and shaved. A small 1.5 cm longitudinal incision was made on the ventral side, and four different gel-scaffold complexes were inserted into individual subcutaneous pockets. The skin incision was closed with sutures.

Characterization of Implanted Scaffolds: At 2 weeks post implantation, mice were perfused under heavy, near-lethal level of anesthesia with 4% isoflurane in 2 L/min oxygen. First, PBS containing 0.1 mg/ml heparin sulfate was injected into the left ventricle to exsanguinate via the cut inferior vena cava. Then mice were perfused with PBS containing fluorescent microbeads (Invitrogen) for micro-angiography.[31] Scaffolds were subsequently harvested and analyzed for mRNA expression by qRT-PCR, β-galactosidase activity by x-gal staining, angiogenesis by micro-angiography and CD31 staining, and the presence of remaining GHPA gel and general histological analysis by trichrome staining.

Gene Expression Analysis via Quantitative Polymerase Chain Reaction (qRT-PCR): Samples were homogenized in Trizol (Invitrogen), and RNA was collected using RNeasy kit (Qiagen). RNA concentration and 260/280 ratios were measured on a TECAN M1000 plate reader. RNA was treated with DNAse to eliminate genomic contamination, and reverse-transcribed using High Capacity cDNA Synthesis Kit (ABiosystems). SYBR Green PCR mix (Biorad) was used for quantitative PCR. Each

sample containing at least 40 ng cDNA and 500 nM of each primer with annealing temperature at 55°C was run in technical triplicates, followed by melting curve analysis. Raw data were analyzed using CFX Manager (Biorad), and biological replicates from different animals were combined.[41] GAPDH expression was used as a reference gene, where the GAPDH expression level divides each gene expression level for normalization. This relative gene expression to GAPDH is then normalized to that of the control condition. Primers used in this study are listed in Table 1.

Table 4.1. List of RT-PCR primers used in this study.

Genes	Forward Primer	Reverse Primer	Accession
ANGPT1	TCACTCAGTGGCTGCAAAAACTTG	CTAGCAGTTGTATTTCAAGTCGGG	NM_001286062.1
ANGPT2	CACAGTGGCTGATGAAGCTGG	GTCGTCTGGTTTAGTACTTGGGC	NM_007426.4
CD31	TCCCTGGGAGGTCGTCCAT	GAACAAGGCAGCGGGGTTTA	NM_008816
Flk1	GAGAGCAAGGCGCTGCTAGC	GACAGAGGCGATGAATGGTG	NM_010612
GAPDH	TGAAGCAGGCATCTGAGGG	CGAAGGTGGAAGAGTGGGAG	NM_001289726
iNOS	CCAAGCCCTCACCTACTTCC	CTCTGAGGGCTGACACAAGG	NM_010927
MRC-1	TTGTGGTGAGCTGAAAGGTG	GTGGATTGTCTTGTGG	NM_008625
MyoD	AGGCTCTGCTGCGCGACC	TGCAGTCGATCTCTCAAAGCACC	NM_010866.2
Myogenin	CCAGGAGATCATTTGCTCG	TTCTGGACATCAGGACAGCC	NM_031189.2
NFL	CCAGGAAGAGCAGACAGAGGT	GTTGGGAATAGGGCTCAATCT	NM_010910.1
NFM	ACCAGGACACCATCCAGCAG	GCTGTCGGTGTGTGTACAGAGG	NM_008691.2
NSE	AGCGTTACTTAGGCAAAGGTGT	AGATACCTGAGCTGATGAGGGC	NM_013509.2
Tie1	ACCCACTACCAGCTGGATGT	ATCGTGTGCTAGCATTGAGG	NM_011587.2
Tie2	GCCTTAATGAACCAGCACCAAG	CCTTATAGCCTGTCCTCGAAC	NM_001290549.1
Trk-A	GCAGCCACCGTGAAGAAAT	GCACCAATGATGCTGCTCCA	NM_001033124.1
VE-cadherin	TCCTCTGCATCCTCACCATCACA	TAAGTGACCAACTGCTCGTGAAT	NM_009868
VEGFA	ATGCGGATCAAACCTCACCA	CCGCTCTGAACAAGGCTCAC	NM_001110267.1
vWF	GCTTGAACTGTTTGACGGAGAGG	TGACCCAGCAGCAGGATGAC	NM_011708

Tissue Preparation for Immunohistochemistry: Samples were fixed in 4% paraformaldehyde (PFA) for 24 hours at 4 °C, washed with PBS, and immersed in 5%-30% sucrose solution until samples sank. Samples were then embedded in Optimal Cutting Temperature compound (TissueTek) and frozen in acetone and dry ice bath. 5 μm-thick sections were obtained by cryosectioning.

Trichrome Green Staining: Trichrome green staining for implanted GHPA gel cryosections was performed by the Vanderbilt Research Histology Core.

β-Galactosidase Staining: Sample cryosections as well as positive and negative controls were fixed with 4% PFA for 10 min at room temperature, washed with PBS, and incubated at 37°C for 2 days in a solution containing the following: 27 mM NaH_2PO_4, 73 mM Na_2HPO_4, 2 mM $MgCl_2$, 2 mM EGTA, 1 μg/ml NP40, 5 mM $K_4[Fe(CN)_6]$, 5 mM $K_3[Fe(CN)_6]$, and 1 mg/ml x-gal (all chemicals from Sigma-Aldrich). Slides were then washed with dH_2O and mounted for imaging.

Immunostaining: Samples were fixed with 4% PFA for 10 min at room temperature, washed with PBS, blocked with 10% goat serum and 0.1% Triton-X100 overnight at 4°C, washed with PBS, and incubated with 1:100 goat anti-mouse CD31 antibody (sc-1505, Santa Cruz Biotechnology), 1:100 rabbit anti-LacZ antibody (ab616, Abcam), 1:100 rabbit anti-Flk1 antibody (sc-504, Santa Cruz Biotechnology) for 2 hours, followed by incubation with 1:1500 IR680LT-conjugated anti-rat antibody (92668029, Licor) and ReadyProbes® AlexaFluor 488-conjugated anti-rabbit antibody (R37116, Invitrogen). Sections were then counter-stained with DAPI and mounted for imaging.

Imaging: Bright-field microscopy for β-galactosidase and trichrome green stain was performed on a Nikon Eclipse Ti microscope, and fluorescence images for immunostaining and micro-angiography were acquired using a Zeiss 710 confocal laser microscope. ImageJ (National Institutes of Health, USA) was used for all image preparation and analysis, including z-stacking fluorescence images and quantification.

Statistical Analysis: Results are presented as means ± standard deviation (SD) or standard error mean (SEM) as indicated. Comparisons among different conditions were performed via ANOVA, followed by Tukey's HSD test in Prism 6 (Graphpad). For all statistics, $p < 0.05$ was considered statistically significant, and such significance is indicated where appropriate.

4.3 Results and Discussion

Gelatin-Hydroxyphenyl Propionic Acid (GHPA) Synthesis and Characterization

Injectable and sprayable hydrogels were successfully produced from hydroxyphenyl propionic

acid-conjugated gelatin that underwent in situ oxidative crosslinking among the phenolic moieties catalyzed by HRP in the presence of H_2O_2 (Figure 4.1A and B). As seen in Figure 4.1B, two GHPA solutions were prepared in order to avoid premature gelation where one GHPA solution contains HRP with cells, and the other GHPA solution contains H_2O_2. HRP/cells- or H_2O_2-containing GHPA solutions are loaded into separate syringes, and the solutions can be injected or sprayed for in situ cross-linking towards mimally-invasive in vivo applications.[19] ^{1}H NMR and UV-vis spectra of GHPA and unmodified gelatin in Figure 1C and D confirmed successful conjugation with 145.1 μmol HPA/g total polymer.

Figure 4.1. (A) Synthesis of gelatin-hydroxyphenyl propionic acid (GHPA). (B) Rapid gelation of GHPA by H_2O_2 and horseradish peroxidase (HRP)-catalyzed oxidative crosslinking. Bottom right image shows a dual-syringe system for cell-containing GHPA injections for in situ crosslinking, and this system can be used for injection or spraying. (C) ^{1}H NMR and (D) UV-vis spectra of synthesized GHPA and unmodified gelatin.

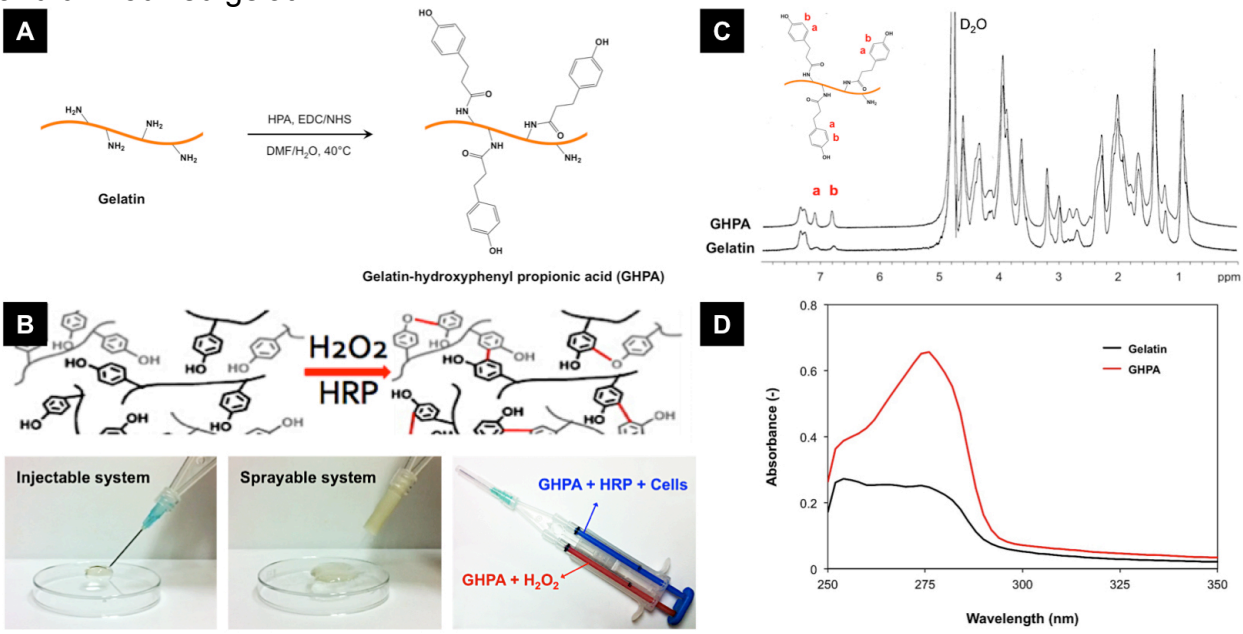

Mechanical properties were characterized without cells at 37°C in wet conditions. All test samples underwent complete gelation within 20 seconds and their storage moduli (G') were measured at varying GHPA and H_2O_2 concentrations (Figure 4.2). Overall, crosslinked GHPA gels exhibited storage moduli ranging from ~100 Pa to ~2500 Pa which are typical of soft hydrogels

and similar to native tissue.[20] As GHPA and/or hydrogen peroxide concentration(s) increased up to 7% and 0.01% (w/v) respectively, the storage modulus increased due to enhanced crosslinking. A previous study demonstrated a similar relationship wherein the resistance to degradation correlated directly with crosslinking density.[19] Three different formulations (arrows in Figure 4.2) were chosen for the cell experiments, each with different mechanical properties. Conditions with storage moduli < 500 Pa were excluded from the selection, as these soft gels were difficult to handle and degraded within a few days, even in in vitro cell cultures.

Figure 4.2. Storage moduli (G') of crosslinked GHPA gels with varying concentrations of GHPA [%w/v] and H_2O_2 [%w/v] were measured using a rheometer with N=5 and error bars = +1 SEM. The compositions indicated with arrows were used for the following biological experiments.

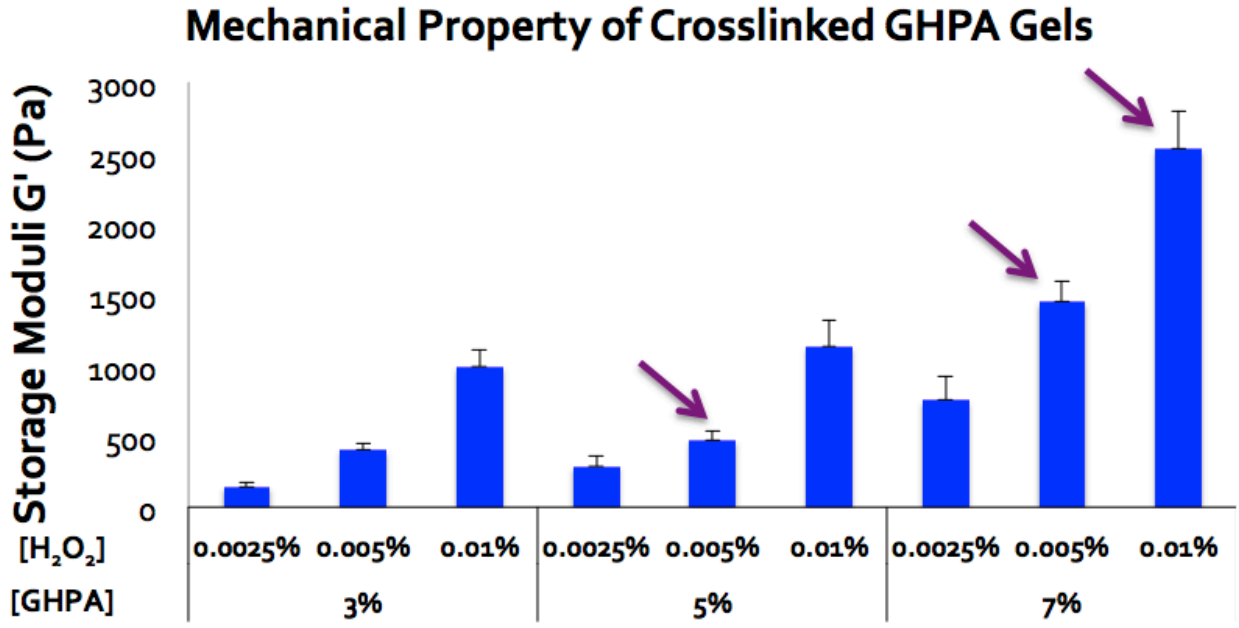

In Vitro 3D Culture of Mesenchymal Stem Cells (MSCs) in GHPA

Using the dual-syringe system, GHPA solutions containing MSCs, HRP, and/or H_2O_2 were mixed upon injection and gelled in a 24-well plate of tissue culture polystyrene (TCPS) for 15 days of in vitro 3D culture. Reduction of resazurin was used as an indicator of live metabolic cells to measure viabiliity on days 1, 7, and 15 (Figure 4.3A).[21] Among the different GHPA compositions, there were

no statistical differences in cell viability, although the condition with the highest GHPA and H_2O_2 contents (7%:0.01%) exhibited a slight decrease in viability. Hydrogen peroxide, a known cytotoxic agent, may account for the low viability at 1 and 7 days as well as the retarded growth in 7%:0.01% condition compared to other compositions.[22] In addition, inefficient diffusion of nutrients and wastes inherent in 3D static culture may also have negatively affected the cell viability.[23] Despite its shortcomings at the early culture period, viability of MSCs in GHPA gels greatly improved to around 80% for all GHPA conditions by day 15.

Figure 4.3. (A) In vitro cell viability of MSCs encapsulated in crosslinked GHPA gels on days 1, 7, and 15 compared to MSCs on tissue culture polystyrene (TCPS) by resazurin reduction with N=3 and error bars = ±1 SD. X%:Y% denotes X %w/v gelatin and Y %w/v H_2O_2. (B) Z-stacked confocal images of Live/Dead stained 3D MSC culture in GHPA on days 1, 7, and 15.

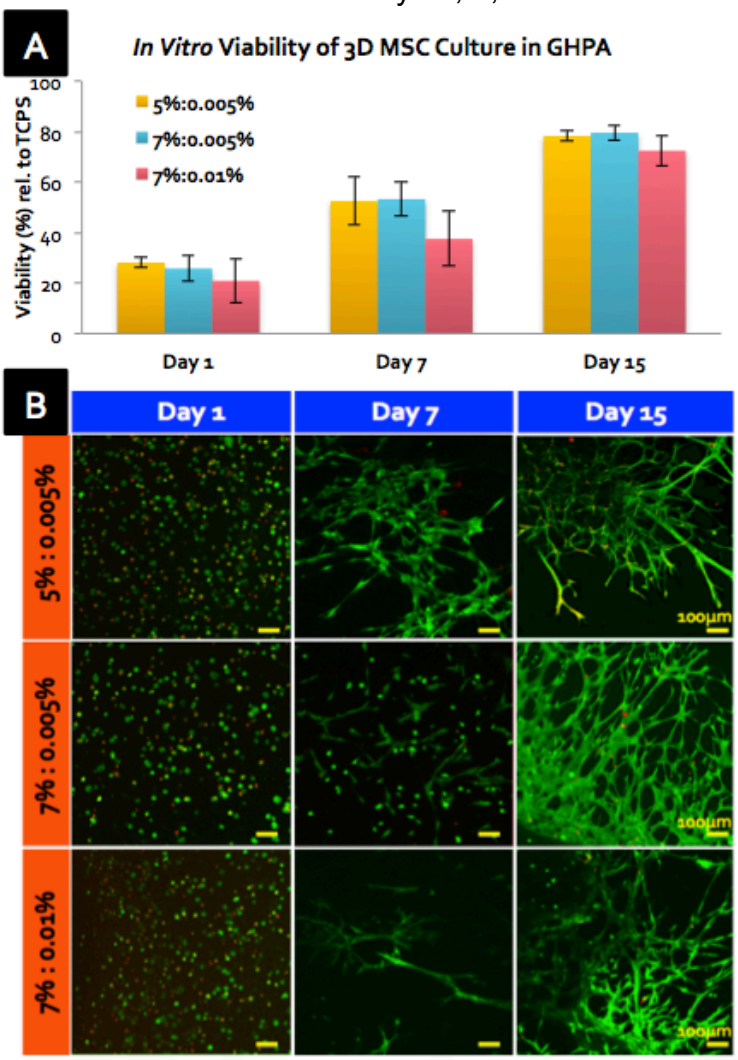

As a collagen-derived material, gelatin possesses numerous cell binding recognition sites with the RGD sequence being the most well-studied and prevalent site.[24] This is a crucial advantage of collagen- or gelatin-based materials over synthetics (ie. poly(ethylene glycol) hydrogels) whose cell attachment relies critically on tethered molecules with reduced viability.[25] Most anchorage-dependent cells require attachment and spreading on a culture substrate for survival and proliferation, and poor cell attachment usually results in a rounded cell morphology and death due to anoikos.[26] The improved cell viability and healthy cell morphology upon 3D encapsulated culture were also evidenced in live/dead imaging over time (Figure 4.3B). MSCs appeared rounded yet viable at day 1; by day 7, most cells began extending through the gel, and by day 15 the cells formed highly-branched networks within the gel, while the top surface of GHPA gel was completely covered by a confluent cell monolayer (data not shown). Overall, crosslinked GHPA gels supported robust MSC viabilty and proliferation within and on the surface of the material, likely due to the favorable properties derived from collagen. Furthermore, changes in cell morphology and organization into unusual, highly-branched networks not only demonstrated active cell-material and cell-cell interactions, but led to question if MSCs began to differentiate within the GHPA gels.

In Vitro MSC Differentiation to Endothelial Lineage in GHPA

Since the organization of branched networks was observed in MSCs encapsulated in GHPA gels on day 15 in vitro (Figure 4.3B), we tested the ability of the material to promote MSC differentiation to specific lineages. An initial differentiation survey was performed by RT-PCR for several myogenic (MyoD, Myogenin), neuronal (NSE, Trk-A, NFL, NFM), and endothelial (VEGFA, CD31, Flk1, ANGPT1, ANGPT2, Tie1, Tie2, VE-cad, vWF) markers. Among the markers investigated, the expression of eight vascular-endothelial lineage markers was significantly up-regulated, compared to the TCPS control (Figure 4.4A). Of note, MSCs in all conditions were positive for a neuronal marker NSE, and GHPA gels promoted very weak expression of Trk-A. However, no significant up-regulation in expression of neuronal markers in MSCs cultured in GHPA gels was

observed relative to TCPS control, while the expression of eight vascular-endothelial markers were clearly up-regulated. Importantly, MSCs in all GHPA gels demonstrated de novo expression of critical, endothelial-specific markers, such as Tie2, ANGPT1, VE-Cadherin, and vWF, that are only observed in MSCs when stimulated with meticulous treatment with bioactive molecules or in co-culture with endothelial cells.[13,44]

Hence, we decided to further characterize potential MSC differentiation into an endothelial lineage in vitro. First, quantitative RT-PCR (qRT-PCR) for CD31 and Flk1/VEGFR-2 showed remarkable up-regulation of CD31 (> 5 fold) and Flk1 (≈ 4 fold) expression in comparison to MSCs cultured on TCPS ($p < 0.05$) (Figure 4.4B). Subsequently, MSCs stained positive for Flk1 and CD31 in all crosslinked GHPA conditions (Figure 4.4C), compared to non-detectable levels of CD31 and Flk1 expression in TCPS control (Figure 4.4D). These results demonstrate the causal role of GHPA on in vitro MSC differentiation into the endothelial lineage at both the gene and protein levels. Furthermore, F-actin staining of MSCs in GHPA gel revealed clear lumen formation as shown in Figure 4.4E.

Previous studies employing similar gelatin materials have shown that gels < 600 Pa in stiffness promoted neuronal differentiation while stiff gels > 8000 Pa promoted myogenic differentiation of human mesenchymal stem cells in vitro with the use of mitomycin.[42,43] Taken together, our results suggest that GHPA gels with stiffness in the range of 600 ~ 2500 Pa have potential to promote MSC differentiation towards an endothelial lineage in vitro. Existing literature shows that cell binding to the RGD sequence on gelatin or denatured collagen involves integrin αvβ3, which is also found to cross-talk with Flk1, thereby promoting proliferation, migration and tubulogenesis of endothelial cells.[24, 27] Additionally, blocking of αvβ3 is proven to be an effective way to restrict angiogenesis as an anti-cancer therapy, signifying the necessity and importance of αvβ3 in angiogenesis.[28] Hence, prevalent RGD ligands on GHPA likely promoted endothelial differentiation and subsequent angiogenenesis by the MSCs via the αvβ3-Flk1 mechanism, which is in agreement with the previous works.[27, 29]

Elucidating the exact mechanism of inducing endothelial differentiation and tubulogenesis from MSCs by crosslinked GHPA gels is a major subject of our next study.

Figure 4.4. (A) Expression for vascular-endothelial, myogenic, and neural lineage markers in MSCs was determined from mRNA after 15 days of culture in GHPA gels by RT-PCR. + indicates positive controls from heart (vascular-endothelial), skeletal muscle (myogenic), and brain (neural) tissues, while TCPS indicates control MSCs cultured on on tissue culture poly styrene. (B) Expression for endothelial cell markers CD31 and Flk1 in MSCs was determined from mRNA after 15 days of culture in GHPA gels by qRT-PCR with N=3 and error bars = ±1 SEM. * indicates $p<0.05$ in comparison to the control MSCs on tissue culture plate. (C) CD31, Flk1 and nuclei were stained and imaged after 15 days of culture in GHPA gels, and a merged image for the TCPS control is shown in (D). Z-stacked confocal images are shown in (C). (E) F-actin staining of MSCs after 15 days of culture in 7%:0.005% condition showed clear lumen formation. Insets contain orthogonal views.

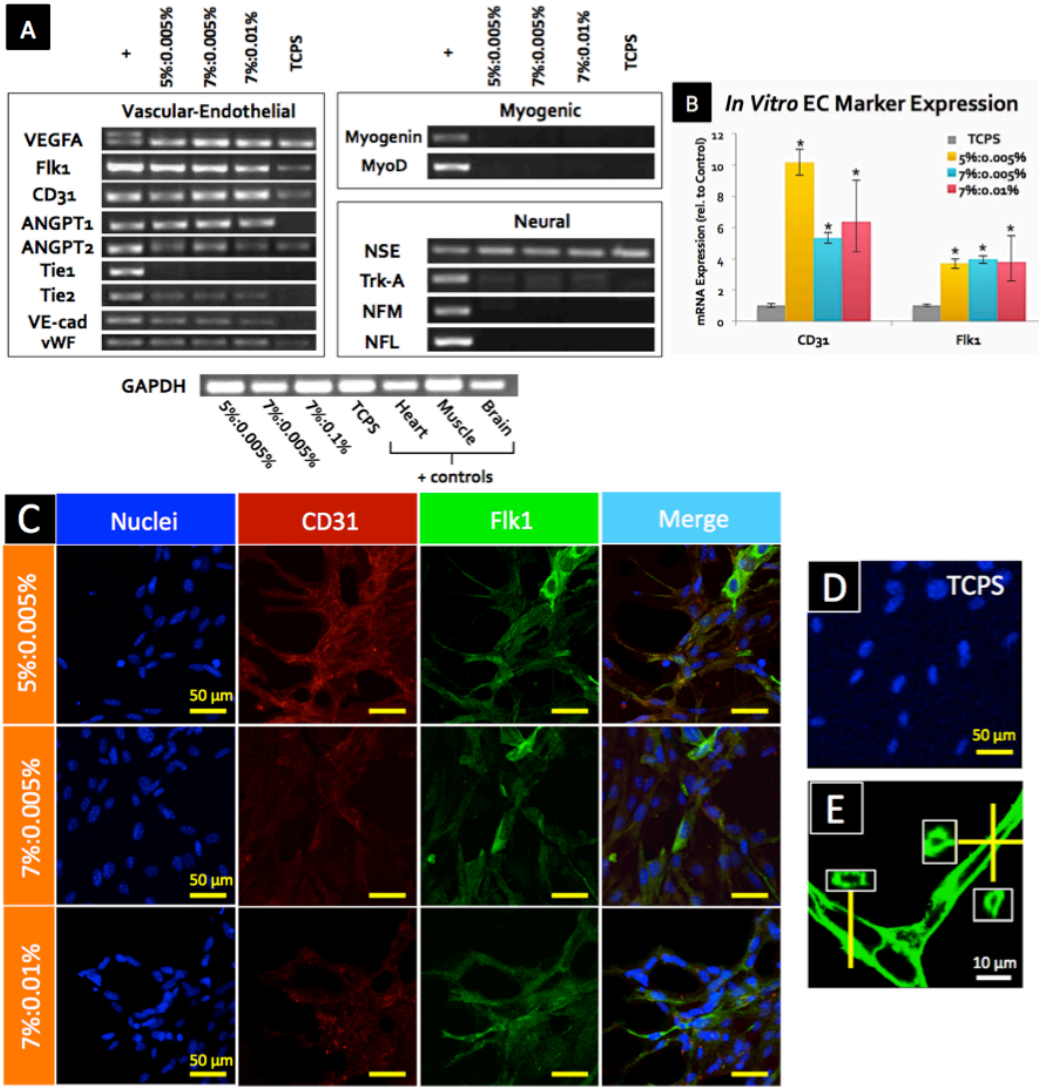

In Vivo Delivery, Engraftment and Tracking of MSCs in GHPA Gels

In order to confirm the effect of GHPA gels on MSCs in vivo, Flk1-LacZ MSC-containing GHPA gels were injected into porous, non-biodegradable polyvinyl alcohol (PVA) sponges to allow for the tracking of delivered cells and GHPA as a target organ model.[30] Multiple gel-PVA sponge complexes were implanted into the ventral subcutaneous regions of wild type mice for 2 weeks (Figure 4.5A). Flk1, the murine analogue to human KDR/VEGFR2, is a well-established marker of vasculature and considered to be endothelial cell-specific. Therefore, Flk1-LacZ MSCs that begin expressing Flk1 in these experiments can be detected with β-galactosidase staining, and are indicative of endothelial differentiation. Flk1-LacZ transgenic MSCs were used to track and distinguish the implanted cells from host wild type cells, and provided a convenient reporter system for monitoring MSC differentiation into endothelial cells.

After 2 weeks of implantation, the scaffolds were harvested for analyses. Trichrome green staining was used to visualize newly-formed collagen or injected GHPA (green-light blue), cytoplasm of various cell types (purple-red), and erythrocytes (small pink rings due to the lack of nuclei) (Figure 5B). In all test conditions, there was robust leukocyte infiltration throughout the scaffolds, and groups of erythrocytes were often observed as well. However, there were two significant differences among the conditions: 1) more collagen and/or GHPA was present throughout the scaffolds in the conditions with higher GHPA and hydrogen peroxide contents, and sometimes lumps of the remaining GHPA were observed in crosslinked GHPA conditions (e.g. lower left corner in the upper image of 7%:0.01% condition in Figure 4.5B), and 2) crosslinked GHPA conditions exhibited extensive vascular networks throughout the scaffolds, with organized branches of cells extending a few hundred microns and containing erythrocytes which indicates functional, perfused vasculature, while the control condition lacks such structures (e.g. images in the lower panel of Figure 4.5B). Additionally, it was evident that there were no giant foreign body cells or fibrous capsule formation around the injected gels, indicating the non-inflammatory nature of GHPA. Hence, the conjugation of hydroxyphenyl propionic acid to

geatin likely retains the non-immuno/antigenicity inherited from gelatin.

β-galactosidase staining revealed increasing numbers of the implanted Flk1-LacZ+ MSCs (blue) retained in crosslinked GHPA conditions at 2 weeks post injection, indicating differentiation of the implanted MSC into Flk1/VEGFR2+ endothelial lineage in vivo (Figure 4.5C and D). In particular 7%:0.01% and 7%:0.005% showed 4- and 3-fold increases in Flk1+ MSCs, respectively, compared to the control for which PVA scaffolds were loaded with a non-crosslinked GHPA solution containing Flk1-LacZ MSCs and HRP but without H_2O_2 for implantation. This result confirms that GHPA promotes MSC differentiation into an endothelial lineage in vivo as well as in vitro, and that crosslinking of the GHPA gel is necessary to drive this event.

In Vivo Angiogenesis and Endothelial Differentiation of MSCs Delivered in GHPA

In order to visualize the functional neovasculature in the implanted scaffolds, mice were perfused with heparinized saline containing fluorescent microbeads for micro-angiography before harvesting the scaffolds.[31] The resulting micro-angiograms from the surface and cross-sections of the scaffolds for each condition are shown in Figure 4.6A and quantified in Figure 4.6B. All angiograms presented are from the same mouse. Neovasculature in implanted scaffolds can be distinguished from the vasculature in the native host tissues around the implantation site in two important ways: 1) implanted scaffolds were not as profusely vascularized as the surrounding host tissues, and 2) neovasculature inside or on the surface of the scaffolds were irregular and tortuous in shape, while the vasculature in the neighboring host tissue exhibited well-organized vessel networks running straight and parallel to each other. Across all conditions, the surface of the implanted scaffold showed well-connected and higly-branched vasculature where smaller capillaries with diameters < 10μm sprouted from larger arterioles that were 20-30μm in diameters. The control scaffold also formed a considerable amount of neovasculature on its surface.

Although there were no statistically significant differences among the crosslinked GHPA conditions, there appeared to be a trend indicating an increase in the blood vessel formation on the

surface of the crosslinked GHPA conditions with the higher GHPA content and crosslinking. The crosslinked GHPA conditions, especially the 7%:0.01% condition showed a 100% increase in angiogenesis on the surface compared to the uncrosslinked control. On the other hand, the micro-angiograms from the cross-sections of the scaffolds revealed greater differences between the uncrosslinked control and crosslinked GHPA conditions: the control condition showed a limited degree of neovasculature at the perimeter of the scaffold while the crosslinked GHPA gels supported

Figure 4.5. (A) Schematic of in vivo experiment where Flk1-LacZ MSCs-containing GHPA was injected into and crosslinked within a porous PVA scaffold for a murine ventral subcutaneous implantation. (B) Trichrome green staining of cross-sections of scaffolds at 2 weeks post implantation where cytoplasm is stained red, erythrocytes pink and collagen/GHPA gels blue/green. (C) β-galactosidase staining shows that delivered Flk1-LacZ transgenic MSCs were retained and became Flk1-LacZ+(blue) post 2-week implantation in crosslinked GHPA conditions. The boxes indicate Flk1-LacZ+ cell-containing areas. (D) Quantification of retained MSCs that differentiated into an endothelial phenotype (Flk1-LacZ+ cells) post 2-week implantation with error bars = ±1 SEM and N=4. Statistical significance with $p < 0.05$ is indicated with * in comparison to the control, and **O** in comparison to 5%:0.005%. (B-C) Top row images with scale bars = 200μm, and bottom row images with scale bars = 50μm.

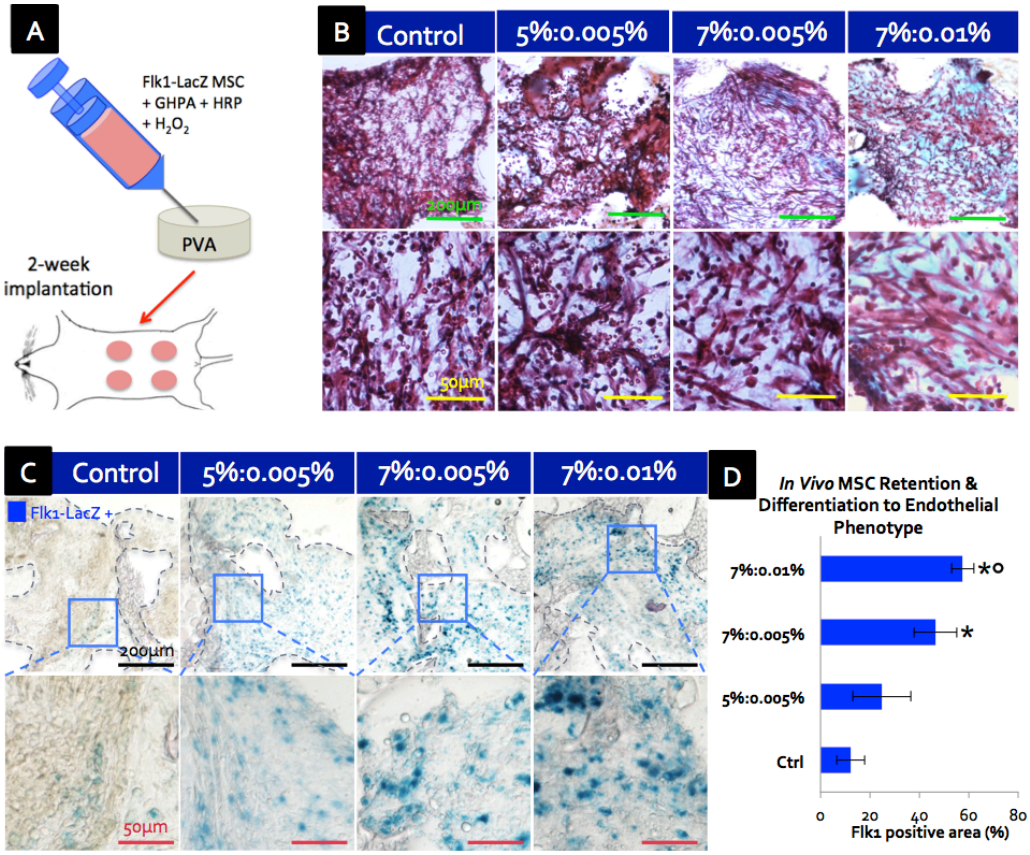

robust angiogenesis throughout the cross-sections. Quantification showed more than 200% increase in all three crosslinked GHPA conditions compared to the control. Understandably, there is less vasculature seen in the cross-sections than on the surfaces due to reduced access, and blood vessels exhibited even more tortuosity within the scaffold, likely due to the physical obstacles driven by the non-biodegradablity of PVA scaffold.

Interestingly, there also appeared to be a positive correlation between the amount of neovasculature and the degree of GHPA content and crosslinking (Figure 4.6B). This implies that the stability of GHPA gels in vivo is a crucial factor in promoting angiogenesis, as uncrosslinked gelatin is known to degrade rapidly in vivo by matrix metalloproteases.[32] Additionally, the tubulogenic effect observed in in vitro experiments was lost in non-crosslinked GHPA control condition in vivo, while the condition containing the most GHPA with the highest level of crosslinking showed the highest degree of angiogenesis among the test groups.

Finally, simultaneous staining of LacZ and CD31 confirmed that Flk1-LacZ+ MSCs were incorporated into the blood vessels (Figure 4.6C). Immunostaining for LacZ yielded similar results to the β-galactosidase staining in Figure 5C, with only few weakly Flk1-LacZ+ MSCs detected in the control condition. For the crosslinked GHPA conditions, numerous cells stained positive for LacZ, however, LacZ expression was the strongest at and co-localized with the CD31+ blood vessels, indicating that the delivered MSCs indeed differentiated into endothelial cells and formed blood vessels in vivo.

Taken together, the angiograms and co-staining of LacZ and CD31 showed branched, perfused neovasculature formation throughout the implanted scaffolds for crosslinked GHPA conditions with clear co-localization between delivered Flk1-LacZ+ MSCs and several CD31+ blood vessels, confirming MSC differentiation into endothelial cells with the aid of crosslinked GHPA in vivo as well as in vitro.

Figure 4.6. (A) Angiograms of the harvested scaffolds by perfusion with fluorescent microbeads at 2 weeks post implantation. Representative images from the outer surface and cross-sections are shown with scale bars = 300 μm. White dotted line marks the boundaries of the scaffolds. (B) % area of the functional blood vessels by angiograms in (A) with error bars = ±1 SEM and N=4. * indicates statistical significance with $p < 0.05$ in comparison to the control. (C) CD31, LacZ and nuclei staining of the cross-sections of the explanted scaffolds with scale bars = 50 μm. All images were acquired by confocal microscopy, and z-stacked.

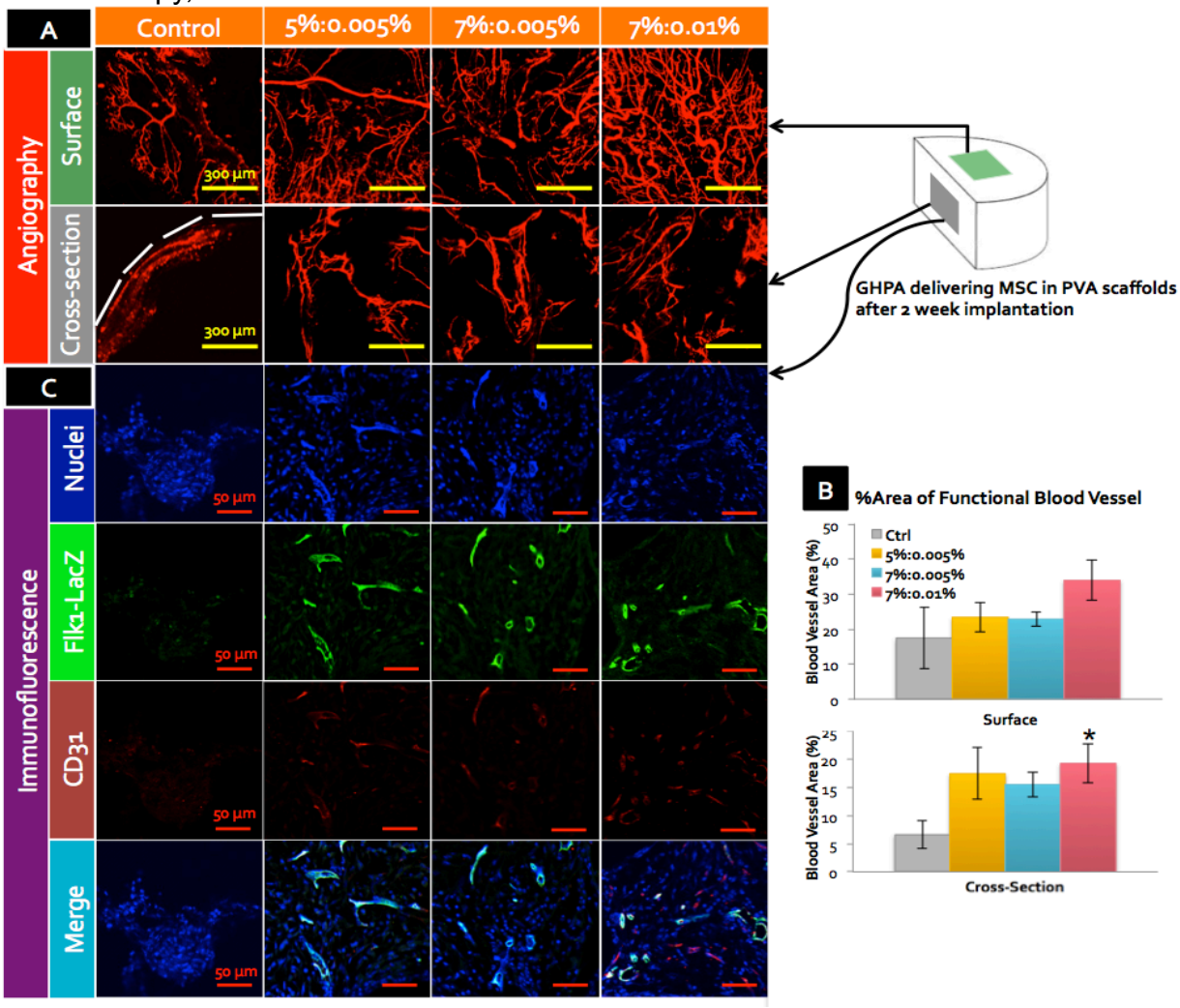

In Vivo Gene Expression in GHPA Gels Delivering MSCs

The gene expression from the harvested scaffolds was analyzed by qRT-PCR. Several markers (Flk1, VE-cadherin, CD31, vWF) for angiogenesis were analyzed (Figure 4.7A). All angiogenic markers surveyed were significantly up-regulated in all crosslinked GHPA conditions compared to the uncrosslinked control. For Flk1 expression, crosslinked GHPA conditions showed approximately 1-, 2-, 3-fold increases in expression for 5%:0.005%, 7%:0.005%, and 7%:0.01%,

respectively. For VE-cadherin expression, crosslinked GHPA conditions showed approximately 1-, 4-, and 12-fold increases in expression for 5%:0.005%, 7%:0.005%, and 7%:0.01%, respectively. In a similar trend, CD31 expression showed 1-, 1-, and 3-fold increases for 5%:0.005%, 7%:0.005%, and 7%:0.01%, respectively. There was a clear positive correlation between the angiogenic marker expression and the GHPA content/crosslinking density, and these results are in agreement with the angiograms and CD31 staining. For vWF expression, however, all crosslinked GHPA conditions had 60% increase in comparison to the control condition. Collectively, these results demonstrate that overall there were significant increases in the expression of angiogenesis markers in the crosslinked GHPA conditions, and that such increases were even more pronounced in conditions with higher amounts of GHPA and crosslinking.

The expression of two markers (iNOS and MRC1) that represent the host macrophage response to the implants were also measured (Figure 4.7B). iNOS expression is associated with a classically-activated/inflammatory macrophage phenotype, while MRC1 expression is regarded as a marker for an alternatively-activated/reparative macrophage phenotype.[33] For iNOS expression, the 5%:0.005% showed a 50% increase compared to the control; however, iNOS expression for 7%:0.005% did not change, and 7%:0.01% showed a 50% decrease in comparison to the control. For MRC1, there was again a GHPA/crosslinking-dependent trend of increasing expression, with 7%:0.01% condition having the highest level of MRC1 expression at 1.9-fold that of the control. These results indicate that the 7%:0.01% condition invoked a favorable response from the host macrophages with reduced inflammation and increased a reparative macrophage phenotype, and this group also demonstrated the highest degree of vascularization and endothelial marker expression, all of which may forecast better long-term integration with the host tissues and functional vascularity. It is also possible that such positive interactions between crosslinked GHPA and host immune cells may have contributed to the increased angiogenesis seen in the crosslinked GHPA conditions since angiogenesis and inflammation are known to be coupled, interdependent processes

Figure 4.7. After 2-week subcutaneous implantation, explanted scaffolds were assayed for gene expression of (A) angiogenesis/ endothelial cell markers and (B) macrophage markers by qRT-PCR with N=4 and error bars = ±1 SEM.

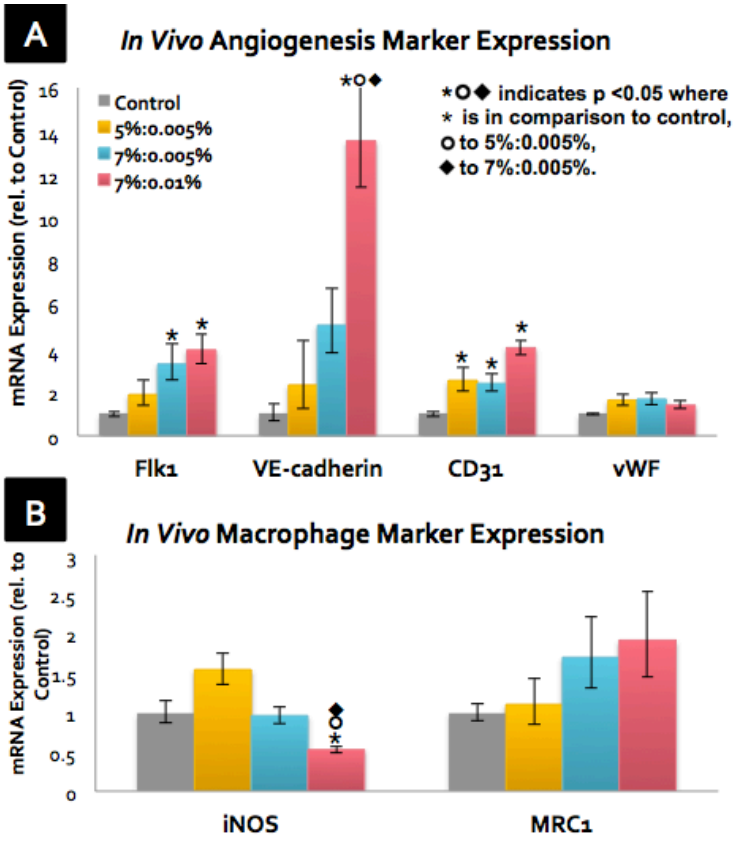

4.4 Conclusion

In this study, injectable and in situ crosslinkable gelatin demonstrated excellent biocompatibility, tunable mechanical properties, and a marked pro-angiogenic effect by promoting endothelial differentiation of MSCs, resulting in robust neovasculature formation throughout the implants, as well as favorable macrophage responses. Previous studies have shown MSC differentiation into endothelial cells using soluble factors such as VEGF and/or bFGF in vitro and/or in vivo.[1-3] In contrast, currently there is only one other study showing differentiation of adipose tissue-derived MSCs into endothelial cells by encapsulating MSCs in PEGylated fibrin hydrogels.[34] In contrast to our study, MSCs in PEGylated fibrin hydrogels did not show increase in Flk1 expression, which implies that there may be multiple mechanisms responsible for endothelial differentiation of MSCs. Nevertheless, our GHPA can be considered as a unprecedented injectable biomaterial platform that

is equipped with advanced functions to direct endothelial differentiation of BM-derived MSCs both in vitro and in vivo via purely material-driven signaling pathways. Such biomaterial-driven stem cell differentiation would be preferred to soluble factor-mediated differentiation due to the reproducibility, relatively economic production cost, reduced spatiotemporal variations commonly observed in soluble factor treatments, minimized side effects, and the physical and instructive support provided for tissue regeneration at the target site. The results are also highly significant as this is one of the first studies to use a purely gelatin-based material in the form of an injectable hydrogel for vasculogenic delivery of stem cells in the fields of tissue engineering and regenerative medicine, which has been almost impossible to-date.

Another important advantage of gelatin-based material is its non-immuno/antigenicity in vivo, as the harsh gelatin extraction process is thought to remove known antigens existing on intact 3D collagen fibrils.[35] Injections of unmodified gelatin into several animals has also failed to produce antibodies.[36] Similarly, past studies involving crosslinked gelatin substrates showed negligible inflammation and no sign of scarring or fibrous capsule formation when implanted, and these results are in agreement with the data presented here.[37-39]

Only a small number of studies have investigated angiogenesis using thermally- or chemically-crosslinked, pre-fabricated solid gelatin scaffolds, and these studies often used clinically-available hemostatic agent Gelfoam®. These studies showed significant angiogenesis in the implants, even when implanted alone.[37, 38] Interestingly, it was also shown that crosslinked gelatin scaffolds significantly improved angiogenesis as compared to collagen scaffolds prepared in a similar method.[37] Our study is also in support of the in vivo pro-angiogenic effect of crosslinked gelatin, however, our results are convoluted by the inclusion of highly trophic MSCs.

Due to the ease of isolation and high capacity for ex vivo expansion, BM-derived MSCs represent a highly desirable candidate cell type for in vivo regeneration of vascularized host tissue. However, results from multiple clinical trials demonstrated that the promise of BM-derived cell therapy

has fallen short due to two major obstacles: poor long-term engraftment of cells within the ischemic, hostile wound environment, and poor vascularization. Therefore, our study has focused on overcoming the major hurdles of utilizing easily-obtained BM-MSCs for vascular applications by optimizing a minimally-invasive, targeted delivery strategy, ensuring long-lasting survival and retention of implanted cells post delivery, and promoting angio/vasculogenesis in vivo. In order to strive towards clinical translation, the angiogenic effects of crosslinked gelatin material alone and especially in comparisons to other materials need to be investigated further. In addition, because of the short history of using gelatin-based materials in tissue engineering applications, the exact mechanisms for improved angiogenesis by GHPA and 3D gelatin-cell interactions remain to be elucidated. Further studies are required to better understand the apparent and numerous advantages of GHPA and its optimal applications in specific biomedical fields.

4.5 References

[1] A. Zieris, S. Prokoph, K. R. Levental, P. B. Welzel, M. Grimmer, U. Freudenberg, C. Werner, Biomaterials 2010, 31, 7985.

[2] L. L. Chiu, M. Radisic, Biomaterials 2010, 31, 226.

[3] J. J. Moon, J. E. Saik, R. A. Poche, J. E. Leslie-Barbick, S. H. Lee, A. A. Smith, M. E. Dickinson, J. L. West, Biomaterials 2010, 31, 3840.

[4] E. Dawson, G. Mapili, K. Erickson, S. Taqvi, K. Roy, Advanced drug delivery reviews 2008, 60, 215.

[5] R. L. Juliano, S. Haskill, The Journal of cell biology 1993, 120, 577.

[6] H. K. Kleinman, D. Philp, M. P. Hoffman, Current Opinion in Biotechnology 2003, 14, 526.

[7] S. F. Badylak, D. O. Freytes, T. W. Gilbert, Acta biomaterialia 2009, 5, 1.

[8] M. P. Alfaro, S. Saraswati, P. P. Young, Vitamins and hormones 2011, 87, 39.

[9] M. P. Alfaro, P. P. Young, Cell transplantation 2012, 21, 1065.

[10] S. Saraswati, D. L. Deskins, G. E. Holt, P. P. Young, Wound repair and regeneration : official publication of the Wound Healing Society [and] the European Tissue Repair Society 2012, 20, 185.

[11] J. Wagner, T. Kean, R. Young, J. E. Dennis, A. I. Caplan, Curr Opin Biotechnol 2009, 20, 531.

[12] Y. Cao, Z. Sun, L. Liao, Y. Meng, Q. Han, R. C. Zhao, Biochemical and biophysical research communications 2005, 332, 370; G. V. Silva, S. Litovsky, J. A. Assad, A. L. Sousa, B. J. Martin, D. Vela, S. C. Coulter, J. Lin, J. Ober, W. K. Vaughn, R. V. Branco, E. M. Oliveira, R. He, Y. J. Geng, J. T. Willerson, E. C. Perin, Circulation 2005, 111, 150.

[13] J. Oswald, C. Werner, Stem Cells 2004, 22, 377.

[14] J. W. Liu, S. Dunoyer-Geindre, V. Serre-Beinier, G. Mai, J. F. Lambert, R. J. Fish, G. Pernod, L. Buehler, H. Bounameaux, E. K. Kruithof, Journal of thrombosis and haemostasis : JTH 2007, 5, 826.

[15] C. H. Wang, T. M. Wang, T. H. Young, Y. K. Lai, M. L. Yen, Biomaterials 2013, 34, 4223.

[16] K. J. Portalska, N. Groen, G. Krenning, N. Georgi, A. Mentink, M. C. Harmsen, C. van Blitterswijk, J. de Boer, Tissue engineering. Part A 2013, 19, 2318.

[17] S. Gorgieva, V. Kokol, in Biomaterials Applications for Nanomedicine, (Ed: P. R), InTech, 2011, 17.

[18] H. B. Bohidar, A. Gupta, Biomacromolecules 2005, 6, 1623.

[19] Y. Lee, J. W. Bae, D. H. Oh, K. M. Park, Y. W. Chun, H.-J. Sung, K. D. Park, Journal of Materials Chemistry B 2013, 1, 2407.

[20] A. M. Kloxin, C. J. Kloxin, C. N. Bowman, K. S. Anseth, Adv Mater 2010, 22, 3484.

[21] J. O'Brien, I. Wilson, T. Orton, F. Pognan, European journal of biochemistry / FEBS 2000, 267, 5421.

[22] R. H. Burdon, Free radical biology & medicine 1995, 18, 775.

[23] C. K. Griffith, C. Miller, R. C. Sainson, J. W. Calvert, N. L. Jeon, C. C. Hughes, S. C. George, Tissue engineering 2005, 11, 257.

[24] G. E. Davis, Biochemical and biophysical research communications 1992, 182, 1025.

[25] D. S. Benoit, A. R. Durney, K. S. Anseth, Biomaterials 2007, 28, 66; D. L. Hern, J. A. Hubbell, Journal of biomedical materials research. Part B, Applied biomaterials 1997, 39, 266.

[26] D. E. Ingber, Proc. Natl. Acad. Sci. USA 1990, 87, 3579.
[27] P. C. Brooks, R. A. F. Clark, D. A. Cheresh, Science 1994, 264, 569.
[28] C. Ruegg, G. C. Alghisi, in Angiogenesis Inhibition, (Eds: S. P.M., S. H.J.), Springer, 2010.
[29] P. R. Somanath, N. L. Malinin, T. V. Byzova, Angiogenesis 2009, 12, 177.
[30] G. S. Duncan, T. W. Mak, Journal of immunology 1999, 162, 3022.
[31] A. L. Zachman, S. W. Crowder, O. Ortiz, K. J. Zienkiewicz, C. M. Bronikowski, S. S. Yu, T. D. Giorgio, S. A. Guelcher, J. Kohn, H. J. Sung, Tissue engineering. Part A 2013, 19, 437.
[32] M. S. Agren, British Journal of Dermatology 1994, 131, 634.
[33] A. Sica, A. Mantovani, The Journal of clinical investigation 2012, 122, 787.
[34] G. Zhang, C. T. Drinnan, L. R. Geuss, L. J. Suggs, Acta biomaterialia 2010, 6, 3395.
[35] A. K. Lynn, I. V. Yannas, W. Bonfield, Journal of biomedical materials research. Part B, Applied biomaterials 2004, 71, 343.
[36] W. A. Starin, the journal of infectious diseases 1918, 23, 139.
[37] L. Dreesmann, M. Ahlers, B. Schlosshauer, Biomaterials 2007, 28, 5536.
[38] D. Ribatti, B. Nico, A. Vacca, M. Presta, Nature protocols 2006, 1, 85.
[39] M. S. Ponticiello, F. P. Barry, Journal of biomedical materials research. Part B, Applied biomaterials 2000, 52, 246.
[40] D. L. Deskins, S. Ardestani, P. P. Young, Journal of visualized experiments : JoVE 2012.
[41] E. Willems, L. Leyns, J. Vandesompele, Analytical biochemistry 2008, 379, 127.
[42] L. S. Wang, C. Du, J. E. Chung, M. Kurisawa, Acta biomaterialia 2012, 8, 1826.
[43] L. S. Wang, J. E. Chung, P. P. Chan, M. Kurisawa, Biomaterials 2010, 31, 1148.
[44] T. Menge, M. Gerber, K. Wataha, W. Reid, S. Guha, C. S. Cox, Jr., P. Dash, M. S. Reitz, Jr., A. Y. Khakoo, S. Pati, Stem cells and development 2013, 22, 148

Chapter 5

Aim 3: Elucidating the molecular mechanism driving material-driven endothelial differentiation of mesenchymal stem cells and human mesenchymal stem cell response in GHPA

5.1 Introduction

Our interesting findings from Chapter 4 led to the new phase of the study to investigate the molecular mechanisms behind purely material-driven differentiation of MSCs into endothelial lineage.[1] While there have been a number of previous studies that have shown purely material-driven differentiation of MSCs into osteocytes, neural cells, and chondrocytes, endothelial differentiation most commonly required an extensive use of biochemical agents such as VEGF and FGF, activating the well-characterized VEGF signaling pathway that drives endothelial differentiation in many types of stem cells.[2-4] Interestingly, we also observed an increased expression of VEGF receptor 2 in MSCs cultured in GHPA in the absence of any added growth factors; however, we believe that this must be the result of other mechanisms that led to VEGFR expression. Namely, we suspected that integrins at the cell-material interface are at play in initially driving the differentiation.

Integrins are extracellular matrix receptors expressed on the cell membrane, and they serve as a physical anchoring point for the cell. Additionally, there are a number of different outside-in signaling cascades that could be initiated by integrins upon binding to their ligands. Such outside-in signaling can significantly affect many essential processes such as cell proliferation, death, motility, morphology and differentiation.[5-7] In this preliminary work, we first sought to identify integrins at the MSC-GHPA interface and verify their roles in endothelial differentiation by selectively blocking integrins with inhibitors.

Having observed the material-driven differentiation effects in murine MSCs in aim 2, one of the natural next questions is to examine if the same effects hold in human MSCs. While only about ~300

genes out of ~20,000 are unique to either human or mice as revealed from whole genome sequencing, interspecies differences have been rather difficult to predict and understand at times, as evidenced by countless clinical trials that have ultimately failed after successful pre-clinical studies in mice.[8] Therefore, robust validation in human MSCs is required for translation. To this end, we have isolated bone marrow-derived MSCs from 3 patients, as well as a commercial line from Lonza. In particular, we isolated MSCs from old patients (> 65 years old) as they stand to benefit the most from regenerative medicine approaches. In this preliminary work, we sought to replicate the experiments with murine MSCs from aim 2 with human patient-derived MSCs.

5.2 Materials and Methods

In Vitro 3D Culture of hMSC in GHPA Gels: hMSCs were isolated from the bone marrow of male patients (> 65 in age) free from any blood disorders and cancer. FACS was used to isolate hMSCs that are CD14-/CD20-/CD34-/CD73+/CD90+/CD105+.[9] GHPA and H_2O_2 were dissolved in DMEM media at various % (w/v) as indicated, while a constant concentration of 2.5 μg/ml HRP was used in all conditions. Cells were added to the GHPA+HRP solution at the final concentration of 10^6 cells/ml. The same number of cells was seeded on tissue culture plate without GHPA gel to serve as a control. After GHPA gelled on the well plate, DMEM supplemented with 10% FBS and 1% penicillin-streptomycin was added and media was changed every day over 15 days. For the inhibition study, P11 (EMD Millipore) was used at 10 μM, obtustatin (Tocris Biosciences) at 10 nM, and mVEGF (Sino Biological Inc) at 50 ng/ml as supplements.[10-11]

Western Blotting: Western blot analysis was done according to standard protocols. Primary antibodies used in this study include: ITGA1 (1:200, #10728, Santa Cruz), ITGAV (1:5000, ab179475, Abcam), pAKT (1:1000, #9271S, Cell Signaling) and GAPDH (1:1000, #2118, Cell Signaling). IRdye680- or 800-tagged secondary antibodies (1:8000, Licor) were used, and membranes were imaged in a Licor scanner.

MSC Delivery in GHPA Gels on Polyvinyl Alcohol (PVA) Scaffolds In Vivo: All animal procedures were approved and performed in accordance with Vanderbilt Institutional Animal Care and Use Committee. GHPA and H_2O_2 were dissolved in DMEM media at various % (w/v) as described above, while a constant concentration of 2.5μg/ml HRP was used in all conditions. hMSC ($5x10^5$)-containing GHPA gel solutions in a total volume of 60 μl were loaded on porous 6 mm-diameter PVA scaffolds (Medtronics). As a control, porous PVA scaffolds loaded with non-crosslinked GHPA + HRP gel solution containing h MSCs were implanted. The gel-scaffold complexes were then subcutaneously implanted aseptically on the ventral side of 5-month-old male, immunodeficient NU/J mice (Jackson Lab) for 2 weeks, and the procedure was previously described (Figure 4.5A). Briefly, mice were anesthesized with 1.5 L/min oxygen and 1.5% isoflurane on a warm water blanket, and shaved. A small 1.5 cm longitudinal incision was made on the ventral side, and four different gel-scaffold complexes were inserted into individual subcutaneous pockets. The skin incision was closed with sutures.

Characterization of Implanted Scaffolds: At 2 weeks post implantation, mice were perfused under heavy, near-lethal level of anesthesia with 4% isoflurane in 2 L/min oxygen. First, PBS containing 0.1 mg/ml heparin sulfate was injected into the left ventricle to exsanguinate via the cut inferior vena cava. Then mice were perfused with PBS containing fluorescent microbeads (Invitrogen) for micro-angiography. Scaffolds were subsequently harvested and analyzed for angiogenesis by micro-angiography.

Gene Expression Analysis via Quantitative Polymerase Chain Reaction (qRT-PCR): Samples were homogenized in Trizol (Invitrogen), and RNA was collected using RNeasy kit (Qiagen). RNA concentration and 260/280 ratios were measured on a TECAN M1000 plate reader. RNA was treated with DNAse to eliminate genomic contamination, and reverse-transcribed using High Capacity cDNA Synthesis Kit (ABiosystems). SYBR Green PCR mix (Biorad) was used for quantitative PCR. Each sample containing at least 40 ng cDNA and 500 nM of each primer with annealing temperature at

55°C was run in technical triplicates, followed by melting curve analysis. Raw data were analyzed using CFX Manager (Biorad), and biological replicates from different animals were combined.[41] GAPDH expression was used as a reference gene, where the GAPDH expression level divides each gene expression level for normalization. This relative gene expression to GAPDH is then normalized to that of the control condition.

Imaging: Bright-field microscopy for the inhibition study was performed on a Nikon Eclipse Ti microscope, and fluorescence images for micro-angiography were acquired using a Zeiss 710 confocal laser microscope. ImageJ (National Institutes of Health, USA) was used for all image preparation and analysis, including z-stacking fluorescence images and quantification.

5.3 Results and Discussion

Integrin Expression of mMSCs cultured in GHPA gels *in vitro*

In order to elucidate the integrins involved in material-driven differentiation in murine MSCs, we started by assaying the cultures for various integrin expression through qRT-PCR (Figure 5.1). Of 26 integrins known to date, we focused on known integrins that bind to collagen and others heavily involved in angiogenesis. As expected, the expressions of integrin alpha 1, a collagen receptor, was significantly up-regulated compared to mMSCs grown on tissue culture polystyrene (TCPS). Additionally, integrin alpha v and beta 3, together forming a heterodimer that plays a significant role in angiogenesis, were shown to be up-regulated. Lastly, ERK1 and PI1K that are key downstream signaling molecules in endothelial differentiation were significantly up-regulated as well.

Western blotting was then used to validate the gene expression levels (Figure 5.2A). Surprisingly, the protein level expressions of integrins in many cases did not match our gene level expression assay. However, it has been shown that cells grown 2D on TCPS tend to have un-naturally massive focal adhesion sites rich with integrins with low turn-over compared to the cells cultured in 3D matrix.[12,13] We expect similar effects to be in play. Additionally, we observed

significant up-regulation of pAKT, a key downstream signaling molecule involved in endothelial differentiation, in GHPA conditions. We then examined better negative controls such as mMSCs cultured in alginate gel or PEG hydrogels for 3 days (Figure 5.2B). mMSCs in alginate gel expressed low amounts of integrin alpha 1 and v, as expected, while cells in PEG gels expressed considerable

Figure 5.1. mRNA expression levels of MSCs cultured for 15 days either on tissue culture plate (control) or embedded in 3 different compositions of GHPA (GHPA%:H_2O_2%). Results from 3 biological replicates were used. Error bars = ± SEM, and * indicates statistical significance with $p < 0.05$.

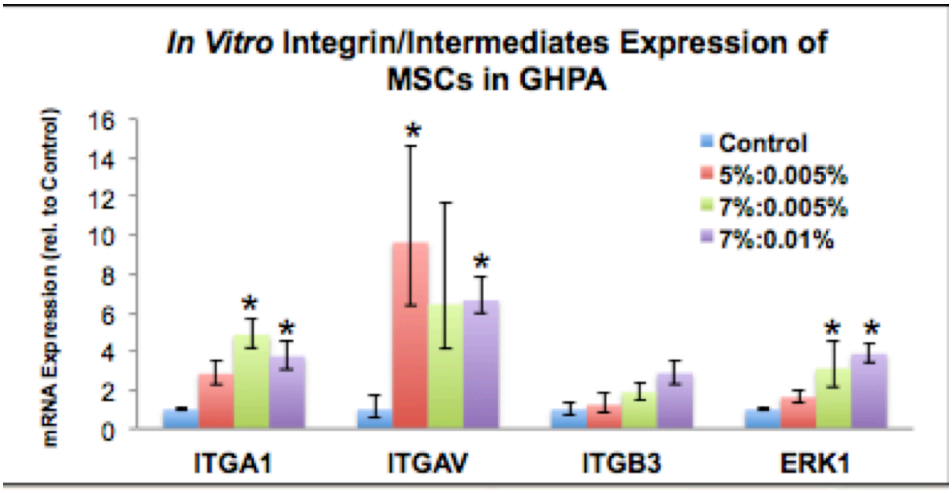

Figure 5.2. Protein expressions of mMSCs were cultured in TCPS and various formulations of GHPA (GHPA%:H2O2%) for 15 days in **(A)** and PEG and Alginate hydrogels for 3 days in **(B)**.

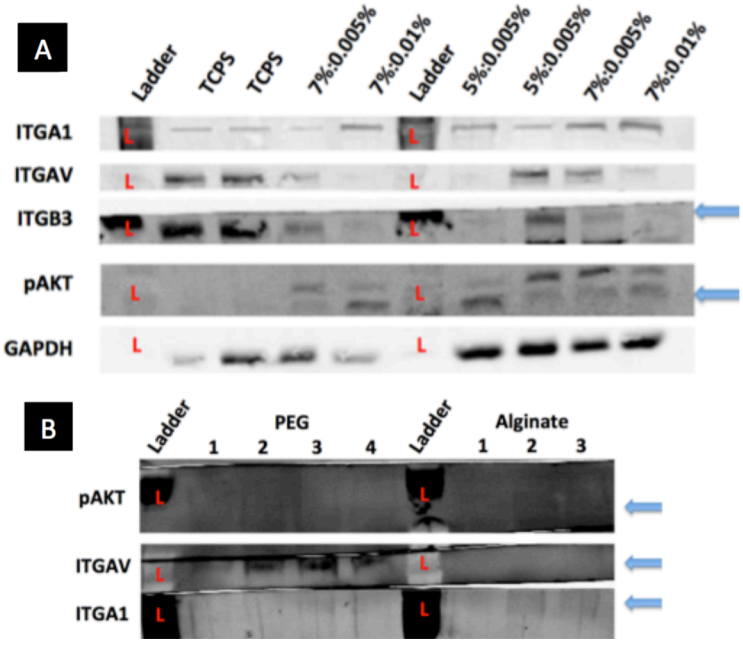

amounts of integrin alpha v and low amounts of alpha 1. In both conditions, mMSCs did not express pAKT. Of note, mMSCs cultured in PEG and alginate gels stayed rounded with complete cell deaths by day 7 (data not shown) due to anoikis. Further work is required to complete the profiling of integrin expression at the protein level using wetern blotting as well as immuostaining to understand how integrins are interacting with the cell matrix.

Inhibition of key integrins attenuates endothelial differentiation

Furthermore, specific integrin inhibitors were used to determine the integrins responsible for driving the endothelial differentiation process (Figure 5.3). Here we added a positive control where soluble VEGF was used in media, as well as two conditions for inhibiting integrins: integrin alpha v/beta 3 inhibitor P11 and integrin alpha 1 inhibitor obtustatin.[10,11] The addition of VEGF visibly improved the amount and connectivity of vasculogenesis in GHPA conditions. Interestingly, both inhibitors appeared to attenuate the material-driven endothelial differentiation, where P11 treated cells stayed rounded through 15 days while obtustatin treated cells tended to aggregate into large clumps and showed limited sprouting activity. These results indicate that integrins alpha v/beta 3 and alpha 1 are crucial in driving endothelial differentiation of mMSCs in GHPA. Further work is required to examine the molecular changes at the gene and protein levels to elucidate the effects of integrin inhibition.

Human MSCs cultured in GHPA *in vitro*

Human MSCs were prepared from bone marrow of three old (> 65 in age) patients via FACS and generously provided by Dr. Pampee Young and Daniel Balikov for this study. Unlike mMSCs, hMSCs did not form extensive tubular network when cultured in 3D GHPA gels (Figure 5.4). Interestingly, hMSCs exhibited better survival through the initial gelling process with most cells surviving throughout the culture period; mMSCs on the other hand exhibited about 30% survival on day 1 (Figure 4.3). Additionally, there is significant underline the many challenges of translating treatment approaches in mice to humans. Several approaches may improve the response in hMSCs,

Figure 5.3. mMSCs cultured on TCPS and GHPA for 15 days with no treatment, soluble VEGF, P11 (integrin alpha v/beta 3 inhibitor) and obtustatin (integrin alpha 1 inhibitor).

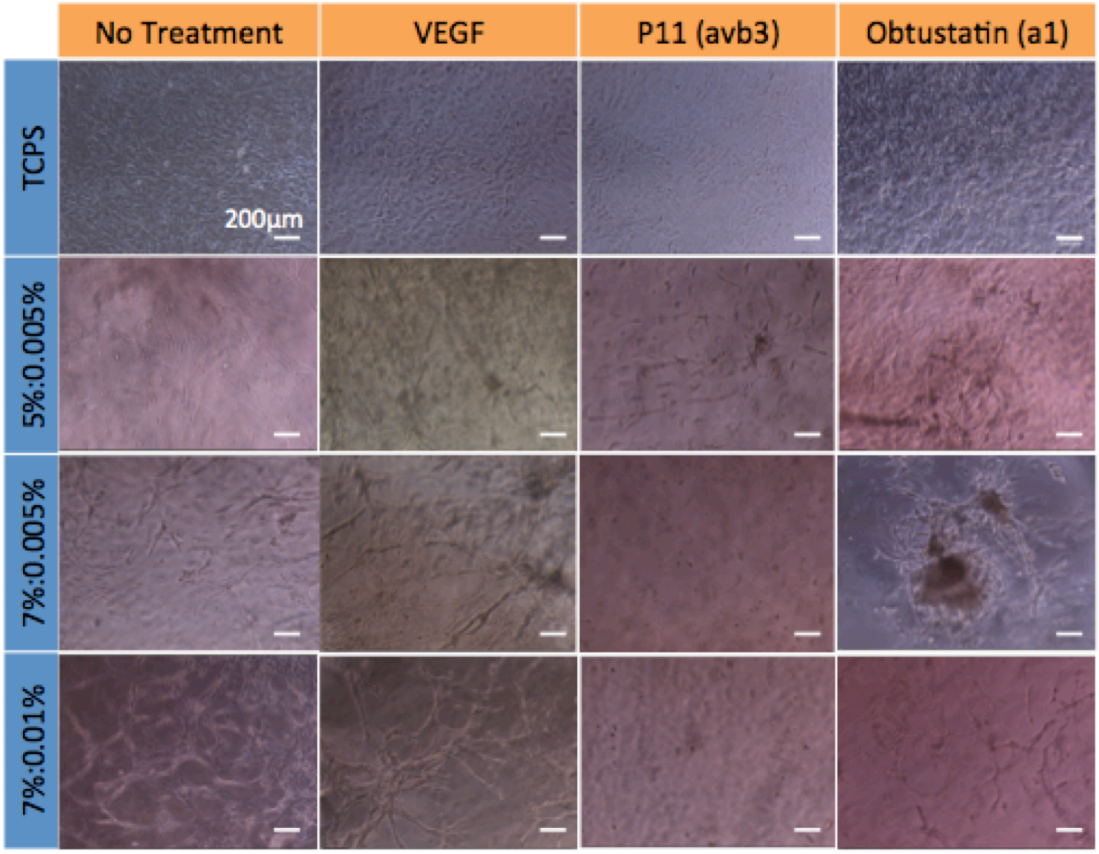

Figure 5.4 Live/dead staining of hMSCs encapsulated in GHPA on day 15 with scale bar = 200 µm

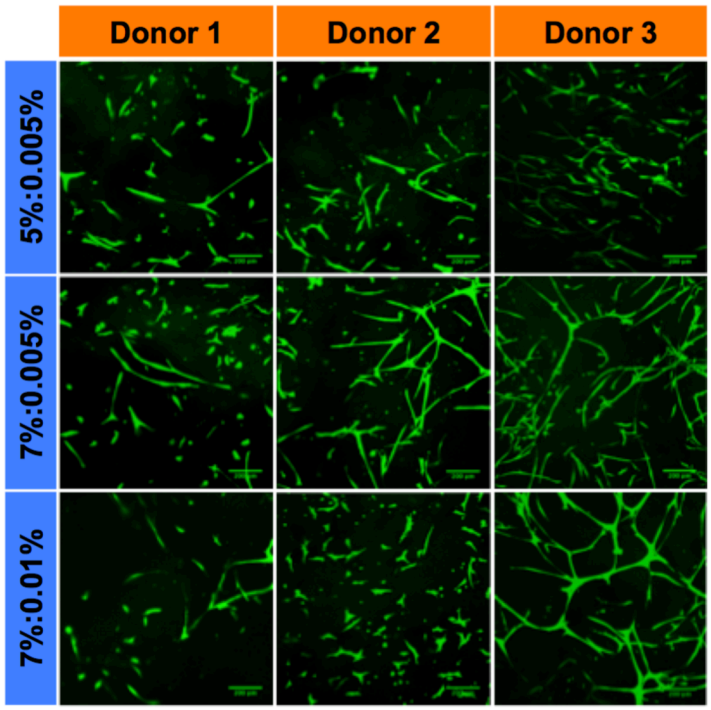

such as the use of VEGF, optimization of cell density, and GHPA formulations among others. Lastly, further verification of endothelial differentiation at gene and protein levels in hMSCs is required.

Angiogenesis in hMSCs delivered in GHPA *in vivo*

To examine if hMSCs in GHPA also induces strong angiogenesis *in vivo* in mice as mMSCs did, we subcutaneously delivered hMSCs in GHPA loaded on PVA scaffolds in an identical setting as was done in chapter 4 with murine cells, except for the use of immunodeficient mice. The use of immunodeficient mice was necessary in order to avoid severe immune response to and eventual rejection of hMSCs in mice. However, it should be noted that immunodeficient mice have severely altered immune system that may poorly model human response.[14] After two weeks of implantation, mice were perfused with fluorescent solution for functional vascular imaging, and the results are shown in Figure 5.5. Overall, we observed increased amounts of vasculature forming for conditions delivering hMSCs in crosslinked GHPA gels compared to the control condition where hMSCs were delivered in non-crosslinked GHPA, similar to what was shown with mMSCs in Figure 4.7. However, we noted 2 key differences: 1) in immunodeficient mice with hMSCs, even control conditions induced angiogenesis throughout the construct while in the mMSC experiment, angiogenesis was limited to the surface area for the control, and 2) in the hMSC experiment, all conditions showed angiogenesis closer to the surface in the cross-sectionals and mostly lacked vascularization in the center. For the first observation, we believe that the altered immune system in immunodeficient mice may have prevented or delayed the formation of fibrous capsule around the control condition, which would have limited vascularization to the surface. For the second observation, it may be attributed to the fact that hMSCs did not undergo significant endothelial differentiation *in vitro* (Figure 5.4) as mMSCs did. Lastly, due to small biological replicates (N=2), the error bars in Figure 5.5B are quite large. It is possible that hMSCs from donor 2 more readily differentiates into endothelial cells and supports angiogenesis *in vivo*. While the results are incomplete, we observed promising trends with hMSC delivery through *in situ* crosslinked GHPA. Similarly, future work would require performing and

Figure 5.5. In vivo angiogenesis in hMSCs delivered via GHPA. Representative confocal images of functional vasculaturere from 2 donor-derived hMSCs shown in **(A)** with blue lines tracing the implants. ImageJ was then used to quantify angiogenesis in **(B)**.

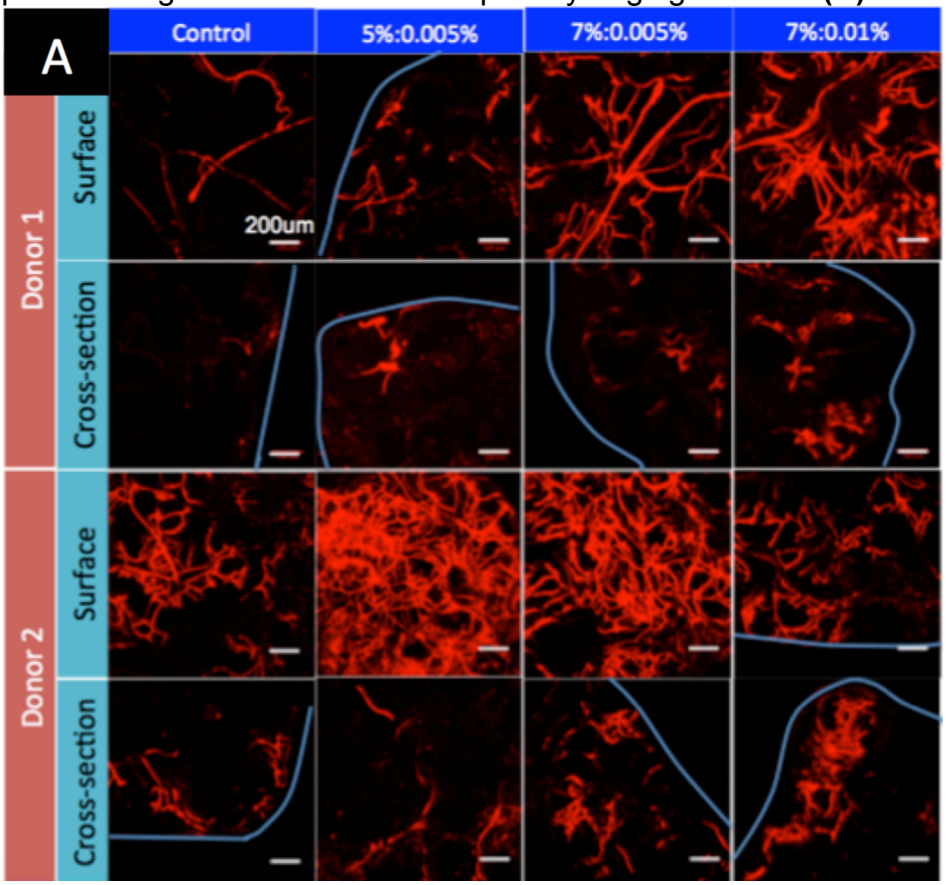

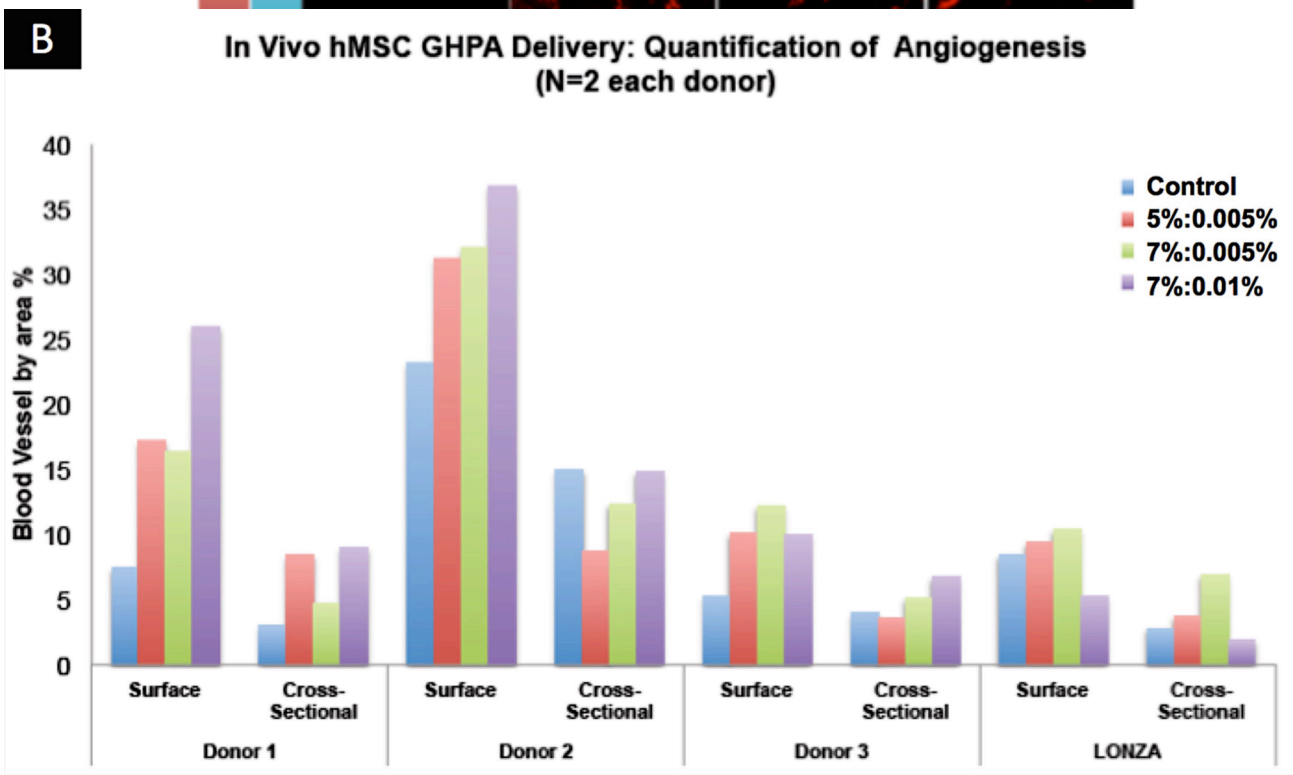

repeating experiments and further analyses at the gene and protein levels.

5.4 Conclusions and Future Directions

While significant work remains to be completed, our preliminary results have identified key integrins necessary for efficient material-driven endothelial differentiation of mMSCs, where the blocking of integrin alpha v/beta 3 and integrin alpha 1 with inhibitors visibly attenuated the hMSC interactions with GHPA to differentiate into endothelial cells. Additionally, We have aimed to take our interesting findings with mMSCs to the next level with hMSCs to assess the translationability of our delivery platform. Our preliminary results from replicating the experiments with patient-derived hMSCs showed that hMSCs by themselves do not sufficiently undergo endothelial differentiation *in vitro*, and their angiogenic effects *in vivo,* while limited in magnitude compared to mMSCs, appear to be strengthened when delivered via crosslinked GHPA. It would be desirable to first optimize the endothelial differentiation process of hMSC in GHPA. For example, the addition of VEGF may successfully drive endothelial differentiation of hMSCs in GHPA gels. Additionally, the next logical experiment would be to apply this platform in a more relevant model, such as the hindlimb ischemia model where therapeutic angiogenic effects could be measured more holistically.

We believe that understanding how MSCs interacts with materials to differentiate into desirable cell types could pave the way for rational design of the next-generation biomaterials that support tissue survival and seamless integration with the host tissues. For example, based on our findings, an even more angiogenic material could be engineered where additional ligands for integrins that were shown to be crucial in endothelial differentiation are presented in the most effective way. While the weak mechanical properties of the GHPA hydrogels as formulated in our studies may not be appropriate for all tissue engineering applications, GHPA may be an excellent material to be used as an element where vascularization is necessary in combination with patient-derived MSCs.

5.5 References

[1] Lee, S. H., Lee, Y., Chun, Y. W., Crowder, S. W., Young, P. P., Park, K. D., & Sung, H. J. (2014). In situ crosslinkable gelatin hydrogels for vasculogenic induction and delivery of mesenchymal stem cells. *Advanced functional materials*, *24*(43), 6771-6781.

[2] Trappmann, B., Gautrot, J. E., Connelly, J. T., Strange, D. G., Li, Y., Oyen, M. L., ... & Spatz, J. P. (2012). Extracellular-matrix tethering regulates stem-cell fate. *Nature materials*, *11*(7), 642-649.

[3] Engler, A. J., Sen, S., Sweeney, H. L., & Discher, D. E. (2006). Matrix elasticity directs stem cell lineage specification. *Cell*, *126*(4), 677-689.

[4] Oswald, J., Boxberger, S., Jørgensen, B., Feldmann, S., Ehninger, G., Bornhäuser, M., & Werner, C. (2004). Mesenchymal stem cells can be differentiated into endothelial cells in vitro. *Stem cells*, *22*(3), 377-384.

[5] Hynes, R. O. (1992). Integrins: versatility, modulation, and signaling in cell adhesion. *Cell*, *69*(1), 11-25.

[6] Hood, J. D., & Cheresh, D. A. (2002). Role of integrins in cell invasion and migration. *Nature Reviews Cancer*, *2*(2), 91-100.

[7] van der Flier, A., & Sonnenberg, A. (2001). Function and interactions of integrins. *Cell and tissue research*, *305*(3), 285-298.

[8] Chinwalla, A.T., Cook, L.L., Delehaunty, K.D., Fewell, G.A., Fulton, L.A., Fulton, R.S., Graves, T.A., Hillier, L.W., Mardis, E.R., McPherson, J.D. and Miner, T.L., 2002. Initial sequencing and comparative analysis of the mouse genome. *Nature*, *420*(6915), pp.520-562.

[9] Bochev, I., Elmadjian, G., Kyurkchiev, D., Tzvetanov, L., Altankova, I., Tivchev, P., & Kyurkchiev, S. (2008). Mesenchymal stem cells from human bone marrow or adipose tissue differently modulate mitogen-stimulated B-cell immunoglobulin production in vitro. *Cell biology international*, *32*(4), 384-393

[10] Marcinkiewicz, C., Weinreb, P. H., Calvete, J. J., Kisiel, D. G., Mousa, S. A., Tuszynski, G. P., & Lobb, R. R. (2003). Obtustatin A Potent Selective Inhibitor of α1β1 Integrin in vitro and Angiogenesis in vivo. *Cancer Research*,*63*(9), 2020-2023.

[11] Choi, Y., Kim, E., Lee, Y., Han, M. H., & Kang, I. C. (2010). Site‐specific inhibition of integrin αvβ3‐vitronectin association by a ser‐asp‐val sequence through an Arg‐Gly‐Asp‐binding site of the integrin. *Proteomics*, *10*(1), 72-80.

[12] Fraley, S. I., Feng, Y., Krishnamurthy, R., Kim, D. H., Celedon, A., Longmore, G. D., & Wirtz, D. (2010). A distinctive role for focal adhesion proteins in three-dimensional cell motility. *Nature cell biology*, *12*(6), 598-604.

[13] Cukierman, E., Pankov, R., Stevens, D. R., & Yamada, K. M. (2001). Taking cell-matrix adhesions to the third dimension. *Science*, *294*(5547), 1708-1712.

[14] Shultz, L. D., Ishikawa, F., & Greiner, D. L. (2007). Humanized mice in translational biomedical research. *Nature Reviews Immunology*, *7*(2), 118-130.

Chapter 6

Significance and Future Directions

6.1 Summary and Significance

In summary, this work was motivated by the unmet clinical needs for tissue engineering to provide necessary organs for the ever-growing patient pool waiting on donated organs. In particular, our work sought to address some of the most pressing challenges in translating tissue engineering into the clinic: namely, the difficulties in vascularizing engineered tissue constructs. To this end, we employed two different approaches to tackle this common barrier. The first approach was to incorporate reactive oxygen species (ROS)-degradable peptide into PCL scaffolds that would allow better cell infiltration, which led to improved angiogenesis. This work is significant, as our study was among the first to apply ROS-sensitive biomaterial for tissue engineering, which has seen extensive applications in drug delivery applications thus far. In the second approach, by modifying gelatin to form a thermostable hydrogel, a novel interaction between gelatin hydrogel and mesenchymal stem cells (MSC) that drove MSC differentiation into blood vessel-forming endothelial cells was discovered and examined. This phenomenon is highly desirable and applicable, as GHPA and patient-derived bone marrow-derived MSCs can be easily obtained and used to support robust microvasculature formation in various engineered tissue constructs. Furthermore, this platform can be easily applied in numerous disease contexts to promote angiogenesis *in vivo* and potentially cure the underlying medical conditions. It is our hope that our studies brought renewed interest in using universally accessible and biofunctional gelatin to promote angiogenesis in tissue engineering for successful implantation and that we demonstrated a successful use of mesenchymal stem cells isolated from the patients as a vascular cell source to form functional vasculature.

Thus, the strengths of our approaches in this work primarily lie in 1) utilizing accessible

materials and cells as well as easy fabrication and application of the developed platforms that could expedite the scale-up and clinical translation/adoption processes, and more importantly 2) illuminating design principles that could be widely applied in tissue engineering. As such, the findings and platforms developed from this work are clinically relevant and translatable. Additionally, the insights gained from our studies add to our understanding of fundamental biological and physiological processes that were previously unexplored. In a way, such novel approaches not only have practical, clinical implications, but they also allow for new biological, physiological questions to be asked and explored. On the other hand, the weaknesses of our work primarily stem from the difficulties in pinpointing the exact mechanisms driving the desirable effects, such as increased cell infiltration, enhanced angiogenesis and MSC differentiation into endothelial cells, due to the innately coupled nature of the variables in each system. Suggestions to address these weaknesses are explored in section 6.2.

Lastly, this work has highlighted the need for an exhaustive and systematic evaluation of various factors within each system, in order to derive universally applicable design principles. It is our belief that elucidating such guiding principles with more clarity would pave the way for tissue engineering to enter the clinic in a timely manner and make a lasting impact on the lives of the patients.

6.2 Future Directions

A significant limitation in this work is the innately coupled nature of the variables within the systems, which makes it difficult to tease out the exact mechanisms for the observed effects. Specifically, in Aim 1, incorporating the ROS-cleavable peptide KP_7K not only resulted in the ROS-degradability of the scaffold as a whole, but it also led to increased cell infiltration, which likely led to enhanced angiogenesis in ROS-degradable scaffolds. Thus, one may ask if the increased cell infiltration and enhanced angiogenesis are due to the ROS-degradability of the scaffolds or to the

non-specific protein-binding motif that KP_7K offers which may facilitate cell binding and migration into the scaffold. One way to decouple these effects would be to introduce antioxidants in the cell culture media, which would scavenge ROS generated from the cells and leave the ROS-degradable KP_7K peptides/scaffold intact. If cell infiltration remains enhanced, then it may mean that the ROS-degradable peptide also inherently promotes cell binding and infiltration due to its protein-binding motif. In the opposite case, it may mean that the cell infiltration is made possible due to the degradation of the scaffold with the concurrent formation of numerous pores that may physically allow better cell infiltration. Decoupling these effects would add valuable insights in designing multifunctional biomaterials.

Similarly, in Aim 2, we observed that culturing MSCs in GHPA gel resulted in the endothelial differentiation of MSCs. While it is clear that the differentiation is purely material-driven by design, it remains uncertain which properties of the material is/are in charge of this desirable effect: mechanical properties, use of H_2O_2 and HRP, certain cell-recognition/binding sites in gelatin or any combination of these factors. It appears likely that the mechanical properties may have an effect on MSC differentiation as many other studies have shown.[4-6] It is also entirely possible that the initial oxidative insult by residual H_2O_2 from crosslinking and the following cell death may have selected for MSCs prone to adapt and differentiate. Lastly, gelatin may present certain cell-binding/recognition sites that may promote MSC differentiation into certain lineages. One way to decouple some of these variables and their effects on MSC differentiation would be to mimic this system with other polymers, such as poly(ethylene glycol) hydroxyphenyl propionic acid to test the effect of gelatin-specific cell-binding sites or to use gelatin hydrogel with an alternate crosslinking method such as the UV-crosslinkable gelatin-methacrylate to test the effect of H_2O_2 and HRP on MSC differentiation. For example, if the PEG-HPA still exerts the same effect on MSCs to differentiate into endothelial cells, then we may rule out gelatin-specific cell-binding sites as the driving force of the differentiation. Similarly, if gelatin-methacrylate also promotes MSC differentiation into endothelial cells without the

use of H_2O_2 and HRP, then we can rule out these crosslinking agents as necessary factors for differentiation. Such exhaustive and systematic evaluation of various factors and decoupling their effects would be instrumental in deriving universally applicable design principles that could significantly advance the field of tissue engineering as a whole, and those principles can be applied in various shapes and forms, tailored to each potential application while delivering the expected outcomes.

Apart from decoupling variables to derive guiding principles, another limiting aspect of this work is the simple subcutaneous implantation rodent model used for our proof-of-concept studies. First, subcutaneous implantation is not a pathophysiologically-relevant model and lacks applicable disease-specific contexts. Since our work showed the improved angiogenesis with ROS-degradable scaffolds in Aim 1 and MSCs delivered in GHPA hydrogels in Aims 2&3, we could further apply these approaches in a more relevant disease model such as the hind limb ischemia model or myocardial infarction model, where enhanced angiogenesis may serve a therapeutic function and significantly improve the outcomes. Secondly, we have used mice for our experiments, however, it is well-known that hundreds of successful therapies in mice have failed to successfully translate in human patients due to a number of interspecies differences, with noticeably different immune systems in rodents vs humans being one significant source of differences.[1] As an example, in Aim 3 we have also observed the drastic differences in how murine MSCs vs human MSCs respond when cultured in GHPA hydrogels. Therefore, in order to better simulate human response future experiments should consider using humanized mice or large animal models in pigs that better mimic human physiology.[2,3]

Our approach is immediately applicable and clinically translatable in that the current form of minimally invasive delivery of MSCs and GHPA itself can be directly applied and tested for therapeutic efficacy in treating various ischemic conditions. Furthermore, our approach can in the future become a part of other tissue engineering applications to address a critical need for rapid

vasculature formation to ensure the survival and proper functioning of the constructs for treating numerous conditions and improving the lives of the patients.

6.3 References

[1] Chinwalla, A.T., Cook, L.L., Delehaunty, K.D., Fewell, G.A., Fulton, L.A., Fulton, R.S., Graves, T.A., Hillier, L.W., Mardis, E.R., McPherson, J.D. and Miner, T.L., 2002. Initial sequencing and comparative analysis of the mouse genome. *Nature*, *420*(6915), pp.520-562.

[2] Meurens, F., Summerfield, A., Nauwynck, H., Saif, L. and Gerdts, V., 2012. The pig: a model for human infectious diseases. *Trends in microbiology*,*20*(1), pp.50-57.

[3] Shultz, L.D., Brehm, M.A., Garcia-Martinez, J.V. and Greiner, D.L., 2012. Humanized mice for immune system investigation: progress, promise and challenges. *Nature Reviews Immunology*, *12*(11), pp.786-798.

[4] Engler, A.J., Sen, S., Sweeney, H.L. and Discher, D.E., 2006. Matrix elasticity directs stem cell lineage specification. *Cell*, *126*(4), pp.677-689.

[5] Reilly, G.C. and Engler, A.J., 2010. Intrinsic extracellular matrix properties regulate stem cell differentiation. *Journal of biomechanics*, *43*(1), pp.55-62.

[6] Wen, J.H., Vincent, L.G., Fuhrmann, A., Choi, Y.S., Hribar, K.C., Taylor-Weiner, H., Chen, S. and Engler, A.J., 2014. Interplay of matrix stiffness and protein tethering in stem cell differentiation. *Nature materials*, *13*(10), pp.979-987.